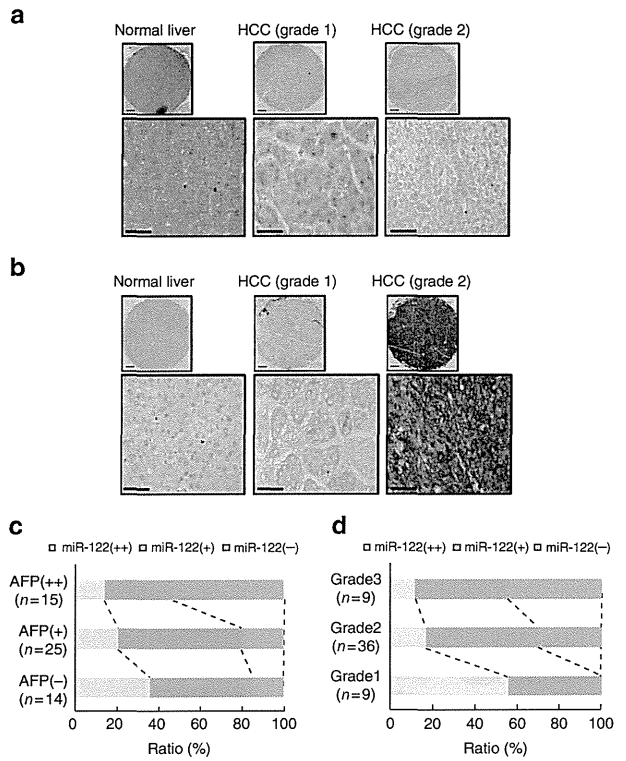

Figure 8 | AFP expression and HCC grade are inversely correlated with miR122 expression in human HCC samples. (**a**) Expression of miR122 in human clinical samples was assessed by *in situ* hybridization. Expression of miR122 (blue/purple staining) in grade 2 (more malignant) HCC samples was less than that of normal human liver tissues or grade 1 (less malignant) HCC samples. Representative images are shown. Nuclei were stained with FastRed. Scale bar, 500 μm. (**b**) AFP expression, shown in brown, was analysed by immunohistochemistry. AFP expression was higher in grade 2 HCC samples than in normal human liver tissue or grade 1 HCC samples in most cases. Representative images are shown. Scale bar, 500 μm. (**c**) Graph shows the correlation between miR122 and AFP expression. Increased AFP expression was correlated with decreased miR122 expression. (**d**) Graph shows the correlation between miR122 expression and malignancy grading of HCC. Increases in malignancy grading were correlated with decreases in miR122 expression.

are frequently observed simultaneously in the clinic: elevated expression of AFP and a more malignant biological phenotype. First, elevated AFP expression and greater cellular invasiveness were observed in miR122-knockdown cells *in vitro* and *in vivo*. Second, CUX1, which is linked with invasive characteristics in carcinoma cells[32,36,37], was shown to be involved in regulation of AFP expression and was identified as a direct target of miR122. Third, in human tissue samples from HCC patients, inverse correlations were observed between miR122 expression and AFP expression, and between miR122 expression and tumour grade. These data suggest that it is unlikely that the clinical correlation between elevated AFP levels and a more biologically aggressive phenotype in HCC is a coincidental epiphenomenon, but, instead provide a possible molecular explanation for the decrease in miR122 expression in HCC cells.

A recent study on liver development reported that liver-enriched transcription factors activate the expression of miR122, which in turn was found to promote terminal differentiation of hepatocytes through the silencing of CUX1 (ref. 42). In the present study, we confirmed that CUX1 is a direct target of miR122 and, in contrast to the situation in normal development, we showed that in grade 2 HCCs the decrease in miR122 is associated with higher CUX1 expression. High CUX1 expression was previously shown to inversely correlate with relapse-free and overall survival in high-grade breast cancers[36]. In transgenic mice, CUX1 was reported to cause various cancer-associated disorders depending on the specific isoform and tissue type expression[34,43–46]. In particular, expression of CUX1 caused organomegaly in several organs including the liver[43]. Hepatomegaly was associated with progression of lesions beginning with inflammation and leading to the development of mixed cell foci, hyperplasia and even HCCs, although in this last case statistical significance was not achieved because of the small size of the transgenic cohort[47]. The underlying mechanisms for the role of CUX1 in cancer is complex and is likely to involve both cell-autonomous and non-cell autonomous effects. However, from cell-based assays it is clear that CUX1 has a role in at least three distinct processes: cell motility, cell cycle progression and chromosome segregation[30,31,36,48]. The knockdown of CUX1 using siRNA was shown to delay entry into S phase and to hinder cell motility and invasion[31,36,48]. In contrast, overexpression of p110 CUX1 was able to accelerate S phase entry and to stimulate proliferation, migration and invasion[35,48]. Moreover, CUX1 was shown to promote genomic instability following cytokinesis failure[30]

Regulation of AFP gene expression is a complex process mediated by a number of transcriptional activators and repressors that bind the AFP gene[7,8]. ZBTB20 was recently identified as a potent repressor of AFP transcription in knockout mouse studies[9]. Our results demonstrate that decreased miR122 expression leads to concomitant decreases in ZBTB20 protein expression. This effect is mediated through upregulation of CUX1, as CUX1 silencing in miR122-silenced cells was shown to lead to both recovery of ZBTB20 levels and reduced AFP expression. Furthermore, the increased expression level of ZBTB20 in CUX1 knockdown cells suggests that ZBTB20 expression is regulated by CUX1. This miR122/CUX1/miR214/ZBTB20/AFP pathway may explain the deregulated AFP expression observed in HCC cells. Additionally, the ability of CUX1 to activate RhoA and to regulate the expression of many proteins involved in cell motility may explain the increased migration and invasiveness associated with malignancy of HCC[31–36]. It should be noted that, although this analysis revealed a trend toward inverse correlation between expression of miR122 and expression of AFP, this correlation could not be applied to all cases examined. Therefore, the possibility of additional pathways that regulate AFP expression cannot be discounted. Nonetheless, our results demonstrate that a decrease in miR122 function is a key factor that contributes to the regulation of AFP expression in HCC.

MiR122 is the most abundant miRNA in the normal adult liver, comprising approximately 80% of all miRNAs[18]. The numerous reported roles of miR122 include regulation of cholesterol biosynthesis[19,20], hepatitis C virus replication[49] and maintenance of the adult liver phenotype[21]. Specific miRNAs are often involved in the differentiation of specific cells and tissues[50]. As miR122 is liver-specific, we reasoned that this miRNA may have a role in the differentiation of normal hepatocytes. In our study, transgenic mice in which miR122 was functionally silenced were found to exhibit elevated AFP levels, but did not display abnormal morphological development in the liver (at least, not up to the age of 12 weeks), suggesting that decreased miR122 expression itself does not cause cells to become transformed. Ongoing characterization of these mice will be required to fully determine the physiological roles of miR122 in the noncancerous liver *in vivo*.

In summary, we have shown that decreased miR122 expression in HCC is linked both to more biologically aggressive tumour behaviour and elevated AFP expression. Furthermore, both of these effects were shown to be mediated by increased expression of CUX1, a direct target of miR122. Similar strategies could also be used to develop new therapeutics and diagnostics for other cancers in which miRNAs that regulate both tumour characteristics and serum markers have been identified.

Methods

Cell culture. The human HCC cell lines, Huh7, PLC/PRF/5, HepG2, Hep3B and Huh1 were obtained from the Japanese Collection of Research Bioresources. The human embryonic kidney cell line, 293T and the human breast cancer cell line HS578T were obtained from the American Type Culture Collection . All cells were maintained in Dulbecco's modified Eagle medium, supplemented with 10% fetal bovine serum.

Mouse experiments. All experiments were carried out in compliance with the regulations of the Animal Use Committee of The University of Tokyo and The Institute for Adult Disease, Asahi Life Foundation.

Generation of transgenic mice in which miR122 was functionally silenced. Mice in which miR122 function was knocked down were generated using previously described protocols[38,51]. Briefly, a DNA fragment of 1,085 bp, containing the H1 promoter region, the coding region for the antisense miR122 stem-loop-stem RNA precursor, and a transcriptional terminator of five thymidines, was resected from the miRZip-122 construct described above by digestion with *Pvu*II. Proper silencing function of the resulting DNA was confirmed via transient transfection-based reporter assays that showed efficient knockdown of miR122 function. Stable C57BL/6 embryonic stem cell lines were generated by electroporation of the linearized transgene, and the resulting cells were injected into blastocysts by the UNITECH Company. Genotyping was performed by PCR using DNA isolated from tail snips. Four different mouse lines were maintained and the male littermates were used in experiments.

Chromatin immunoprecipitation assay. ChIP for CUX1 was performed as previously described[52]. For the scanning ChIP of the miR214 locus, realtime PCR analysis was performed using primer pairs specific for different regions of the promoters. Templates for the PCR reactions were 0.1% total input DNA (I), nonspecific DNA from sepharose beads alone (S), or chipped chromatin. The respective fold enrichment of the different DNA fragments are indicated relative to the DNA obtained by purification on sepharose beads without IgG (S). Enrichment was calculated using the HPRT locus as a reference.

Doxycyclin-induced shRNA against CUX1 system. For conditional knockdown of CUX1 in Hs578t cells, we took advantage of the Addgene plasmid 11643. HS578T cells were infected with pLVCT shCUX1(5,326–5,348)-tTRKRAB lentivirus as described[53]. At 48 h after infection, cells were split and cultured with or without doxycyclin at a final concentration of 2.5 $\mu g\,ml^{-1}$. Cells were used for experiments after 5 days of treatment. Doxycyclin was then removed from the culture media and cells were maintained for 4 days following release.

Cell proliferation assay. Relative cell proliferation was assessed using a Cell Counting Kit-8 (Dojindo Laboratories), as described previously[54].

Enzyme-linked immunosorbent assay. AFP levels in the cell-culture supernatant were examined using an AFP-specific ELISA kit supplied by an outsourcing company, SRL.

Western blot analysis. Protein lysates were prepared from cells or mouse liver for immunoblot analysis. Proteins were separated by SDS–polyacrylamide gel electrophoresis and transferred to polyvinylidene difluoride membranes. After blocking with 5% dry milk to decrease nonspecific binding, membranes were probed with the appropriate primary antibodies. Primary antibodies were obtained from Abcam (ZBTB20, #ab48889, 1:500) and Santa Cruz Biotechnology (CDP, #sc-13024, 1:1,000). CUX1 antibodies (#861, 1:1,000) were generated as described previously[52]. Horseradish peroxidase-conjugated secondary antibodies were used to detect primary antibodies. Bound antibodies were detected using ECL Plus Western blotting detection reagents (GE Healthcare Life Sciences).

Scratch assay. The effects of miR122 knockdown on cellular migratory function were determined by evaluating cellular migration after scratching of a confluent monolayer of cells. Monolayers were cultured on 10 $\mu g\,ml^{-1}$ fibronectin-coated dishes and were scratched using a 200-µl pipette. Migration was analysed at the indicated time points after scratching.

***In vitro* invasion assay**. The effect of miR122 knockdown on invasive function was determined using BD BioCoat Matrigel Invasion Chambers (Becton Dickinson) according to the manufacturer's recommended protocol. Cell invasion was induced by removing the serum in the upper chamber. The number of invading cells was analysed after 22-h incubation. Cell numbers were counted in four randomly chosen fields at each time point.

Quantitative pseudopodia assay. Pseudopodium quantitation was performed using a Quantitative Pseudopodia Assay Kit (Chemicon) according to the manufacturer's instructions. Briefly, the upper chamber was coated with fibronectin and seeded with cells in serum-free medium. Serum was added to the lower chambers. 8 h later, pseudopodia on the lower surface were stained and eluted, and the absorbances of solubilized samples at 600 nm was measured using a microplate reader.

CUX1-knockdown lentiviral construct. Lentiviral particles expressing CUX1 shRNA were purchased from Santa Cruz Biotechnology (#sc-35051-V).

***In situ* hybridization to assess miR122 and miR214**. The expression of miR122 and miR214 in mouse liver and human HCC tissues was examined by *in situ* hybridization[55,56]. Locked nucleic acid (LNA)-scramble (negative control) and LNA-anti-miR122 and LNA-anti-miR214 probes were obtained from EXIQON. After deparaffinization, tissue sections were treated with 10 $\mu g\,ml^{-1}$ proteinase K for 5 min at 37 °C and refixed with 4% paraformaldehyde, followed by acetylation with 0.25% anhydrous acetic acid in 0.1 M Tris–HCl buffer (pH 8.0). Following pre-hybridization for 30 min at 48 °C, hybridization was performed overnight with each 20 nM LNA probe in hybridization buffer (5xSSC buffer, 50% formamide, 500 $\mu g\,ml^{-1}$ tRNA, 50 $\mu g\,ml^{-1}$ Cot-1 DNA). After completion of hybridization, the sections were washed with 0.1×SSC buffer for 10 min at 52 °C three times and blocked with DIG blocking buffer (Roche Diagnostics) for 30 min. Sections were then probed with anti-DIG (1:500; Roche Diagnostics) for 1 h at room temperature. Detection was performed by incubation in NBT/BCIP buffer (Promega) overnight. Nuclei were stained with Nuclear FastRed (Sigma-Aldrich).

Immunohistochemistry. Tissue arrays containing HCC tissues were purchased from US Biomax. To determine the correlations between AFP, ZBTB20, CUX1, miR122 and miR214 expression and HCC differentiation grade, slides carrying consecutive sections were obtained. Slides were baked at 65 °C for 1 h and deparaffinized. Endogenous peroxidase activity was blocked by incubation in 3% hydrogen peroxide buffer for 30 min. Antigen retrieval was performed by incubating the slides at 89 °C in 10 mM sodium citrate buffer (pH 6.0) for 30 min. To minimize nonspecific background staining, slides were blocked in 5% normal goat serum (Dako) for 10 min at room temperature. Tissues were labelled overnight at 4 °C with primary antibodies raised against AFP (Dako, #N1501, 1:100), CUX1 (#sc-13024, 1:100) and ZBTB20 (HPA016815, Sigma-Aldrich, 1:100). Slides were then incubated with anti-rabbit horseradish peroxidase-conjugated secondary antibodies (Nichirei Bioscience) for 1 h. Primary antibody binding was visualized by incubation in 3,3′-diaminobenzidine in buffered substrate (Nichirei Bioscience) for 5 min. The slides were counterstained with haematoxylin, dehydrated with ethanol, and mounted with Clarion mounting medium (Biomeda).

GTP-binding RhoA and Rac1 immunoprecipitation assay. The amount of RhoA activity was examined using an Active Rho Pull-down and Detection Kit (Thermo Fisher Scientific) according to the manufacturer's recommended protocol. The amount of GTP-bound RhoA protein (the active form of RhoA) was detected by Western blotting with the provided anti-RhoA antibody (1:100). Rac1 activity was similarly determined by using PAK-GST Protein Beads (#PAK02, Cytoskeleton) for pulldowns and anti-Rac1 antibodies (1:100) for subsequent Western blotting (#89856D, Thermo Fisher Scientific).

Orthotopic xenograft tumour model of HCC. Male BALB/c (nu/nu) nude mice were purchased from CREA Japan (Tokyo, Japan). The transplantation of tumour cells into mouse livers was performed using previously reported methods[57,58]. Briefly, 2×10^6 control or miR122-silenced PLC/PRF5 cells were suspended in 30 µl of PBS containing 1% Matrigel (Becton Dickinson). After anaesthesia, the liver was exposed through a surgical incision. Cells were slowly injected under the capsule of left lobe of the liver using a 28-gauge needle. When successful, a transparent bleb of cells could be seen through the liver capsule. After injection, light pressure was applied to the injection site with sterile gauze for 2 min to prevent bleeding and tumour cell leakage. The abdomen was then closed with sutures. Transplantation was successful in a total of 12 mice (6/group). At 4 weeks post-transplantation, liver tissues were collected, serially sectioned, and stained with haematoxylin and eosin.

Statistical analysis. Statistically significant differences between groups were determined using Student's *t*-test when variances were equal. When variances were unequal, Welch's *t*-test was used instead. *P*-values less than 0.05 were considered statistically significant.

Plasmid and stable cell line construction, reporter assays, RT–PCR, northern blotting and immunocytochemistry are described in the Supplementary Methods. All primer information is provided in Supplementary Table S1.

References

1. Parkin, D., Bray, F., Ferlay, J. & Pisani, P. Global cancer statistics, 2002. *CA Cancer J. Clin.* **55,** 74–108 (2005).
2. El-Serag, H. Epidemiology of hepatocellular carcinoma in USA. *Hepatol. Res.* **37,** S88–94 (2007).
3. Llovet, J. *et al.* Sorafenib in advanced hepatocellular carcinoma. *N. Engl. J. Med.* **359,** 378–390 (2008).
4. Greten, T. *et al.* Survival rate in patients with hepatocellular carcinoma: a retrospective analysis of 389 patients. *Br. J. Cancer* **92,** 1862–1868 (2005).
5. Greten, T., Korangy, F., Manns, M. & Malek, N. Molecular therapy for the treatment of hepatocellular carcinoma. *Br. J. Cancer* **100,** 19–23 (2009).
6. Di Bisceglie, A. Issues in screening and surveillance for hepatocellular carcinoma. *Gastroenterology* **127,** S104–S107 (2004).

7. Ogden, S. *et al. p53* targets chromatin structure alteration to repress alpha-fetoprotein gene expression. *J. Biol. Chem.* **276,** 42057–42062 (2001).
8. Peng, S. *et al.* High alpha-fetoprotein level correlates with high stage, early recurrence and poor prognosis of hepatocellular carcinoma: significance of hepatitis virus infection, age, p53 and beta-catenin mutations. *Int. J. Cancer.* **112,** 44–50 (2004).
9. Xie, Z. *et al.* Zinc finger protein ZBTB20 is a key repressor of alpha-fetoprotein gene transcription in liver. *Proc. Natl Acad. Sci. USA* **105,** 10859–10864 (2008).
10. Oishi, K. *et al.* Clinicopathologic features of poorly differentiated hepatocellular carcinoma. *J. Surg. Oncol.* **95,** 311–316 (2007).
11. Yamamoto, K. *et al.* AFP, AFP-L3, DCP, and GP73 as markers for monitoring treatment response and recurrence and as surrogate markers of clinicopathological variables of HCC. *J. Gastroenterol.* **45,** 1272–1282 (2010).
12. Matsumoto, Y. *et al.* Clinical classification of hepatoma in Japan according to serial changes in serum alpha-fetoprotein levels. *Cancer* **49,** 354–360 (1982).
13. Lee, R., Feinbaum, R. & Ambros, V. The *C. elegans* heterochronic gene lin-4 encodes small RNAs with antisense complementarity to lin-14. *Cell* **75,** 843–854 (1993).
14. Carrington, J. & Ambros, V. Role of microRNAs in plant and animal development. *Science* **301,** 336–338 (2003).
15. Bartel, D. MicroRNAs: genomics, biogenesis, mechanism, and function. *Cell* **116,** 281–297 (2004).
16. Ambros, V. The functions of animal microRNAs. *Nature* **431,** 350–355 (2004).
17. Lu, J. *et al.* MicroRNA expression profiles classify human cancers. *Nature* **435,** 834–838 (2005).
18. Landgraf, P. *et al.* A mammalian microRNA expression atlas based on small RNA library sequencing. *Cell* **129,** 1401–1414 (2007).
19. Krützfeldt, J. *et al.* Silencing of microRNAs *in vivo* with 'antagomirs'. *Nature* **438,** 685–689 (2005).
20. Esau, C. *et al.* miR-122 regulation of lipid metabolism revealed by *in vivo* antisense targeting. *Cell Metab.* **3,** 87–98 (2006).
21. Gatfield, D. *et al.* Integration of microRNA miR-122 in hepatic circadian gene expression. *Genes Dev.* **23,** 1313–1326 (2009).
22. Yan, D. *et al.* MicroRNA-1/206 targets c-Met and inhibits rhabdomyosarcoma development. *J. Biol. Chem.* **284,** 29596–29604 (2009).
23. Kutay, H. *et al.* Downregulation of miR-122 in the rodent and human hepatocellular carcinomas. *J. Cell. Biochem.* **99,** 671–678 (2006).
24. Coulouarn, C., Factor, V., Andersen, J., Durkin, M. & Thorgeirsson, S. Loss of miR-122 expression in liver cancer correlates with suppression of the hepatic phenotype and gain of metastatic properties. *Oncogene* **28,** 3526–3536 (2009).
25. Tsai, W. *et al.* MicroRNA-122 a tumor suppressor microRNA that regulates intra-hepatic metastasis of hepatocellular carcinoma. *Hepatology* **49,** 1571–1582 (2009).
26. Varnholt, H. *et al.* MicroRNA gene expression profile of hepatitis C virus-associated hepatocellular carcinoma. *Hepatology* **47,** 1223–1232 (2008).
27. Wong, Q. *et al.* MicroRNA-223 is commonly repressed in hepatocellular carcinoma and potentiates expression of Stathmin1. *Gastroenterology* **135,** 257–269 (2008).
28. Sahai, E. & Marshall, C. RHO-GTPases and cancer. *Nat. Rev. Cancer* **2,** 133–142 (2002).
29. Sansregret, L. & Nepveu, A. The multiple roles of CUX1: insights from mouse models and cell-based assays. *Gene* **412,** 84–94 (2008).
30. Sansregret, L. *et al.* Cut homeobox 1 causes chromosomal instability by promoting bipolar division after cytokinesis failure. *Proc. Natl Acad. Sci. USA* **108,** 1949–1954 (2011).
31. Kedinger, V. & Nepveu1, A. The roles of CUX1 homeodomain proteins in the establishment of a transcriptional program required for cell migration and invasion. *Cell Adh. Migr.* **4,** 348–352 (2010).
32. Michl, P., Knobel, B. & Downward, J. CUTL1 is phosphorylated by protein kinase A, modulating its effects on cell proliferation and motility. *J. Biol. Chem.* **281,** 15138–15144 (2006).
33. Seguin, L. *et al.* CUX1 and E2F1 regulate coordinated expression of the mitotic complex genes Ect2, MgcRacGAP, and MKLP1 in S phase. *Mol. Cell Biol.* **29,** 570–581 (2009).
34. Kedinger, V. *et al.* p110 CUX1 homeodomain protein stimulates cell migration and invasion in part through a regulatory cascade culminating in the repression of E-cadherin and occludin. *J. Biol. Chem.* **284,** 27701–27711 (2009).
35. Michl, P. *et al.* CUTL1 is a target of TGF(beta) signaling that enhances cancer cell motility and invasiveness. *Cancer Cell* **7,** 521–532 (2005).
36. Aleksic, T. *et al.* CUTL1 promotes tumor cell migration by decreasing proteasome-mediated Src degradation. *Oncogene* **26,** 5939–5949 (2007).
37. Kunath, T. *et al.* Transgenic RNA interference in ES cell-derived embryos recapitulates a genetic null phenotype. *Nat. Biotechnol.* **21,** 559–561 (2003).
38. Shouval, D. *et al.* Tumorigenicity in nude mice of a human hepatoma cell line containing hepatitis B virus DNA. *Cancer Res.* **41,** 1342–1350 (1981).
39. Nomura, F., Ohnishi, K. & Tanabe, Y. Clinical features and prognosis of hepatocellular carcinoma with reference to serum alpha-fetoprotein levels. Analysis of 606 patients. *Cancer* **64,** 1700–1707 (1989).
40. Johnson, P., Melia, W., Palmer, M., Portmann, B. & Williams, R. Relationship between serum alpha-foetoprotein, cirrhosis and survival in hepatocellular carcinoma. *Br. J. Cancer* **44,** 502–505 (1981).
41. Xu, H. *et al.* Liver-enriched transcription factors regulate microRNA-122 that targets CUTL1 during liver development. *Hepatology* **52,** 1431–1442 (2010).
42. Ledford, A. W. *et al.* Deregulated expression of the homeobox gene Cux-1 in transgenic mice results in downregulation of p27(kip1) expression during nephrogenesis, glomerular abnormalities, and multiorgan hyperplasia. *Dev. Biol.* **245,** 157–171 (2002).
43. Brantley, J. G., Sharma, M., Alcalay, N. I. & Heuvel, G. B. Cux-1 transgenic mice develop glomerulosclerosis and interstitial fibrosis. *Kidney Int.* **63,** 1240–1248 (2003).
44. Cadieux, C. *et al.* Mouse mammary tumor virus p75 and p110 CUX1 transgenic mice develop mammary tumors of various histologic types. *Cancer Res.* **69,** 7188–7197 (2009).
45. Cadieux, C. *et al.* Polycystic kidneys caused by sustained expression of Cux1 isoform p75. *J. Biol. Chem.* **283,** 13817–13824 (2008).
46. Cadieux, C. *et al.* Transgenic mice expressing the p75 CCAAT-displacement protein/Cut homeobox isoform develop a myeloproliferative disease-like myeloid leukemia. *Cancer Res.* **66,** 9492–9501 (2006).
47. Vanden Heuvel, G. B. *et al.* Hepatomegaly in transgenic mice expressing the homeobox gene Cux-1. *Mol. Carcinog.* **43,** 18–30 (2005).
48. Sansregret, L. *et al.* The p110 isoform of the CDP/Cux transcription factor accelerates entry into S phase. *Mol. Cell Biol.* **26,** 2441–2455 (2006).
49. Jopling, C., Yi, M., Lancaster, A., Lemon, S. & Sarnow, P. Modulation of hepatitis C virus RNA abundance by a liver-specific MicroRNA. *Science* **309,** 1577–1581 (2005).
50. Taulli, R. *et al.* The muscle-specific microRNA miR-206 blocks human rhabdomyosarcoma growth in xenotransplanted mice by promoting myogenic differentiation. *J. Clin. Invest.* **119,** 2366–2378 (2009).
51. Zhou, Y. *et al.* Chimeric mouse tumor models reveal differences in pathway activation between ERBB family- and KRAS-dependent lung adenocarcinomas. *Nat. Biotechnol.* **28,** 71–78 (2010).
52. Harada, R. *et al.* Genome-wide location analysis and expression studies reveal a role for p110 CUX1 in the activation of DNA replication genes. *Nucleic Acids Res.* **36,** 189–202 (2008).
53. Szulc, J., Wiznerowicz, M., Sauvain, M. O., Trono, D. & Aebischer, P. A versatile tool for conditional gene expression and knockdown. *Nat. Methods* **3,** 109–116 (2006).
54. Maeda, S. *et al.* Ikappa B kinasebeta/nuclear factor-kappaB activation controls the development of liver metastasis by way of interleukin-6 expression. *Hepatology* **50,** 1851–1860 (2009).
55. Elmén, J. *et al.* LNA-mediated microRNA silencing in non-human primates. *Nature* **452,** 896–899 (2008).
56. Bai, S. *et al.* MicroRNA-122 inhibits tumorigenic properties of hepatocellular carcinoma cells and sensitizes these cells to sorafenib. *J. Biol. Chem.* **284,** 32015–32027 (2009).
57. Yao, X. *et al.* A novel orthotopic tumor model to study growth factors and oncogenes in hepatocarcinogenesis. *Clin. Cancer Res.* **9,** 2719–2726 (2003).
58. Kim, M. *et al.* Generation of orthotopic and heterotopic human pancreatic cancer xenografts in immunodeficient mice. *Nat. Protoc.* **4,** 1670–1680 (2009).

Acknowledgments

This work was supported by Grants-in-Aid from the Ministry of Education, Culture, Sports, Science and Technology, Japan (#22390058, #22590718, #17016016 and #20390204) (to M. Otsuka, Y. Kondo, M. Omata and K. Koike), by Health Sciences Research Grants of The Ministry of Health, Labour and Welfare of Japan (Research on Hepatitis) (to K. Koike), by grants from the Takeda Science Foundation, Astellas Foundation for Research on Metabolic Disorders, Senri Life Science Foundation, the Foundation for Promotion of Cancer Research and the Mochida Memorial Foundation for Medical and Pharmaceutical Research (to M. Otsuka), and by the grant 019389 from the Canadian Cancer Society (to A.N.).

Author contributions

K. Kojima, M. Otsuka and A.N. planned the research and wrote the paper. K. Kojima, A.T., C.V., T.Y., Y. Kondo, Y. Kang and Z.X. performed the majority of the experiments. M.A., N.K., W.Z. and A.N. contributed materials. T.K. and H.Y. supported several experiments. M. Omata and K. Koike supervised the entire project.

Additional information

Supplementary Information accompanies this paper at http://www.nature.com/naturecommunications

Competing financial interests: The authors declare no competing financial interests.

Reprints and permission information is available online at http://npg.nature.com/reprintsandpermissions/

How to cite this article: Kojima, K. *et al.* MiRNA122 is a key regulator of α-fetoprotein expression and influences the aggressiveness of hepatocellular carcinoma. *Nat. Commun.* 2:338 doi: 10.1038/ncomms1345 (2011).

Clinical Translational Research

Oncology

Oncology 2011;80:406–415
DOI: 10.1159/000330734

Received: April 19, 2011
Accepted after revision: June 15, 2011
Published online: August 15, 2011

Identification by Differential Tissue Proteome Analysis of Talin-1 as a Novel Molecular Marker of Progression of Hepatocellular Carcinoma

Hideaki Kanamori[a, b] Takao Kawakami[d, e] Kathryn Effendi[b] Ken Yamazaki[b] Taisuke Mori[b] Hirotoshi Ebinuma[a] Yohei Masugi[b] Wenlin Du[b] Keiko Nagasaka[e] Atsushi Ogiwara[e] Yutaka Kyono[e] Minoru Tanabe[c] Hidetsugu Saito[a] Toshifumi Hibi[a] Michiie Sakamoto[b]

Departments of [a]Gastroenterology, [b]Pathology and [c]Surgery, School of Medicine, Keio University, [d]Clinical Proteome Center, Tokyo Medical University, and [e]Research and Development Division, Medical ProteoScope Company, Tokyo, Japan

Key Words
Tumor progression · Liquid chromatography-tandem mass spectrometry · Immunohistochemistry · Portal vein invasion · Disease-free survival

Abstract
Objective: Hepatocellular carcinoma (HCC) is characterized by a multistage process of tumor progression. This study addressed its molecular features to identify novel protein candidates involved in HCC progression. ***Methods:*** Using liquid chromatography-tandem mass spectrometry, proteomes of 4 early HCCs and 4 non-HCC tissues derived from 2 cases of liver transplant surgery were compared with respect to the separation profiles of their tryptic peptides. Immunohistochemistry was performed on 106 HCC nodules to confirm the results of the proteomic analysis. ***Results:*** Statistical analysis of the profiles selected the peptide peaks differentiating HCC from non-HCC. A database search of the tandem mass spectrometry data from those peptide peaks identified 61 proteins, including a cytoskeletal protein, talin-1, as upregulated in HCC. Talin-1 expression levels in HCC nodules were significantly associated with the dedifferentiation of HCC ($p = 0.001$). A follow-up survey of the examined clinical cases revealed a correlation between talin-1 upregulation and a shorter time to recurrence after resection ($p = 0.039$), which may be related to the higher rate of portal vein invasion in HCCs with talin-1 up-regulation ($p = 0.029$). ***Conclusions:*** Proteomic analysis led to identification of talin-1 as a promising HCC marker. Talin-1 upregulation is associated with HCC progression and may serve as a prognostic marker.

Introduction

Hepatocellular carcinoma (HCC), like other cancers, is characterized by a multistage process of tumor progression [1]. In the initial stage, the damaged liver tissues evolve into small nodular hypercellular lesions called dysplastic nodules (DNs). These precancerous lesions develop into early HCC, defined as small, well-differentiated HCC of vaguely nodular type, and then into progressed HCC, characterized by a distinctly nodular appearance and frequent microvascular invasion. After treatment, early HCC has a longer time to recurrence and a higher 5-year survival rate than progressed HCC [2]. The long-standing confusion in differentiating early HCC from high-

KARGER

Fax +41 61 306 12 34
E-Mail karger@karger.ch
www.karger.com

0030–2414/11/0806–0406$38.00/0

Accessible online at:
www.karger.com/ocl

Michiie Sakamoto, MD, PhD
Department of Pathology
School of Medicine, Keio University
35 Shinanomachi, Shinjuku-ku, Tokyo 160-8582 (Japan)
Tel. +81 3 5363 3764, E-Mail msakamot@sc.itc.keio.ac.jp

grade DN has been minimized since stromal invasion was recognized as a diagnostic indicator for early HCC [3], but hepatocellular changes occurring during malignant transformation are still not well characterized.

Transcriptomic and proteomic analyses are useful techniques for investigating the carcinogenesis of several malignant diseases. Comparison of the gene expression profiles among early and progressed components of nodule-in-nodule type HCCs and corresponding noncancerous liver tissues resulted in identification of heat-shock protein 70 (HSP70) [4] and cyclase-associated protein 2 [5] as molecular markers of HCC. In this study, we performed proteome analysis for direct comparison of the protein composition of early HCC and non-HCC tissues obtained from whole native livers of patients who underwent living donor liver transplantation (LDLT). During the last decade, liquid chromatography (LC) directly coupled with tandem mass spectrometry (MS/MS) has been widely used for high-resolution proteome-wide analysis from a complex protein mixture [6]. The use of an improved LC-MS/MS technology with optimal tissue sampling led us to the identification of a variety of proteins up-regulated in HCC, including talin-1.

Talin-1 is a cytoskeletal protein with a molecular mass of 270 kDa, and has been shown to play a key role in a wide variety of integrin-mediated cellular events [7]. To our knowledge, there has been no report published on the relationship between talin-1 and HCC. We have successfully applied a proteomic approach to native livers of LDLT cases and showed up-regulation of talin-1 during HCC progression.

Materials and Methods

Liver Samples

HCC and noncancerous liver tissues were obtained from HCC patients at Keio University Hospital between 2003 and 2006. This study was conducted with the approval of the Ethics Committee of Keio University School of Medicine. For proteomic analysis, we used fresh whole livers from 2 HCC patients who received LDLT. Both patients had similar clinical backgrounds (males, 49 and 54 years old at the time of surgery, infected with hepatitis C virus) and were referred to Keio University Hospital after transarterial chemoembolization for multiple HCCs and hepatic deterioration into Child-Pugh score C. Immediately after resection of the whole liver, physiological saline including 2,000 units of heparin sodium was infused into the catheterized portal trunk. After confirming visually that the fluid flowing out of the common hepatic artery and the hepatic veins did not contain residual blood, the liver was sliced into 1.5-cm-thick sections with reference to the magnetic resonance imaging. Two samples of early HCC and 2 samples of noncancerous liver tissue were macroscopically separated in 0.5–1.0-cm^3 portions from each of the livers by two experienced pathologists. The noncancerous samples were derived from the areas which were not adjacent to cancerous lesions and did not contain many fibrotic components. A total of 8 liver samples (4 HCCs and 4 noncancerous tissues) were obtained from the 2 cases and kept frozen at −80°C until use. For immunohistochemical analysis, liver samples were obtained by partial hepatectomy or liver transplant surgery, consisting of 106 HCC nodules (13 well-differentiated HCCs including 7 early, 73 moderately differentiated, and 20 poorly differentiated HCCs) and 8 DNs from the total of 91 HCC patients.

Two-Dimensional Liquid Chromatography (2DLC)-MS/MS

The resected tissues were homogenized, and the homogenates were fractionated into phosphate-buffered saline (PBS) soluble and insoluble fractions [8]. An aliquot (50 μg protein) of the soluble fraction was subjected to tryptic hydrolysis in a polyacrylamide gel matrix [8, 9]. The resulting peptide mixture was extracted from the gel matrix and dried under vacuum. Peptide separation and mass measurement were carried out using 2DLC-MS/MS [10]. Briefly, in the first-dimensional strong cation exchange (SCX) LC, the peptides retained in the SCX LC column were eluted by successive injection of ammonium formate solutions (25, 50, 100, 150, 200 and 500 mM). These effluents were mixed serially with an internal standard peptide mixture consisting of 3 synthetic peptides. The second-dimensional reverse-phase (RP) LC was performed in a total 60-min acetonitrile gradient for each of the SCX LC peptide effluents. The RP LC effluent was interfaced with an electrospray ionization source in positive ion mode on an LTQ linear ion trap mass spectrometer (Thermo Fisher Scientific Inc., Waltham, Mass., USA). Protonated peptides were analyzed sequentially for MS/MS in Data-Dependent Scanning mode, consisting of a full-range scan at an m/z range of 450–2,000 and subsequent product ion scans for each of the three most intense ions in the full scan mass spectrum.

Differential Analysis of Peptide Profiles

A peptide separation profile, consisting of the ion signals characterized by RP LC elution time, full scan m/z value and full scan signal intensity was extracted from each of the RP LC-MS/MS data files. Profile compilation was carried out using an in-house program as reported [11]. Here, the signal alignment process was aided by three common signal sets derived from the three peptides spiked into each SCX LC effluent. Following signal alignment, peak detection was performed by searching the compiled signal profile. The intensity of each detected peak is the total of the signal intensities provided from the respective peptide profiles. Student's t test and heat map representation were performed for the ion signals contained in the detected peaks using Spotfire® software (TIBCO Software Inc., Palo Alto, Calif., USA).

For peptide identification, a database search was performed using Mascot® software (Matrix Science Ltd., London, UK) [12]. MS/MS data were searched for corresponding amino acid sequences in a Swiss-Prot database (http://expasy.org/sprot). Each peptide identification item was computationally associated with a profile peak containing the original precursor ion signals. Peptide identifications were considered significant for a Mascot matching score greater than 30. Identified amino acid sequences of peptides were searched for in the Swiss-Prot database to count the identical sequences in the database.

After selection of the peptide identifications under given conditions, these were grouped into each Swiss-Prot protein sequence entry. According to the fold value of signal intensity, these peptide groups were evaluated for quantitative regulation of the corresponding protein molecules. Functional classification of these proteins was based on information described in the Gene Ontology database (http://www.geneontology.org/).

Immunohistochemistry

Immunohistochemical staining was performed on formalin-fixed, paraffin-embedded tissue sections as described previously [13]. Each section was deparaffinized, rehydrated, incubated with fresh 0.3% hydrogen peroxide in methanol for 30 min at room temperature, and then washed in PBS. The sections were autoclaved at 120°C in 10 mM sodium citrate, pH 6.0, for 10 min before incubation with normal horse serum (Vector Laboratories Inc., Burlingame, Calif., USA) for 30 min. The sections were then incubated with a mouse monoclonal antibody against talin-1 (clone TA205; Millipore Co., Billerica, Mass., USA) at a dilution of 1:200 overnight at 4°C, washed with PBS, and incubated with a secondary antibody for 60 min at room temperature. Staining was evaluated by 3 pathologists. Statistical analyses were performed using SAS® software (SAS Institute Inc., Cary, N.C., USA). Disease-free survival curves were calculated from the day of resection using the Kaplan-Meier method (JMP® software, SAS Institute), and the significance of differences in survival rates between the patient groups was calculated by the log-rank test. The results of the immunohistochemical examination were compared with the microarray data of our past study [14] which are accessible from the Genome Medicine Database of Japan (GeMDBJ; https://gemdbj.nibio.go.jp/dgdb/index.do).

Results

Differential Proteome Analysis of the Compiled Peptide Profiles

From each of the 8 liver samples, 2DLC-MS/MS generated 6 peptide profiles for each of 6 salt concentrations of SCX LC (fig. 1a). The profile compilation was performed separately for each set of 6 SCX LC fractions across the 8 tissue samples, followed by peak detection of the compiled signals. From the 6 SCX LC fractions above, we obtained 2,434, 1,912, 1,819, 1,894, 1,725, and 1,533 peaks, respectively, associated with any peptide identifications. All 11,317 peaks were subjected to selection on the basis of the following conditions: (1) A Student's t test p value less than 0.1 for difference of the signal intensities between HCC and non-HCC. (2) At least 1 peptide identification, with a Mascot matching score more than 30, associated with the relevant peak. (3) Peak intensity more than 1% of the maximum peak in a compilation. After selection, the number of candidate peaks was reduced to 283, comprising 390 peptide identifications, allowing more than two significant peptide identifications in each of the selected peaks. The heat map of the 283 peaks shows successful differentiation between HCC and non-HCC (fig. 1b).

Evaluation and Classification of Tumor Marker Candidates for HCC

Following peak selection, 390 peptide identifications associated with the selected peaks were grouped according to the protein names. Of these, 288 peptide identifications were assigned to 111 groups (proteins), whereas the remaining 102 were individual peptides supported by only single peptide identification from one sample. The latter were excluded from the following analysis because of their ambiguity both for identification and quantitation of protein. According to the fold value, i.e. the ratio of HCC to non-HCC on the average signal intensities involved in a peak, these 111 peptide groups were evaluated for the quantitative regulation status of the corresponding protein molecules. When peptides with a greater than 1-fold value accounted for more than 80% in a peptide group, the corresponding protein was considered to be upregulated in HCC. A total of 61 proteins fell into this category. Accounting for less than 20% of the total, 22 proteins were categorized as downregulated. The other 28 groups were not categorized into either set. The 61 upregulated and 22 downregulated proteins were classified further by their functional and topological aspects, based on the Gene Ontology annotations as follows (table 1): 8 cytoskeletal proteins, 7 heat shock proteins (including HSP70 as upregulated in HCC), 5 major blood proteins, 53 enzymes, and 10 other proteins.

Among several categories of proteins, we primarily chose the cytoskeletal proteins for further validation, since it is generally accepted that disorders in cellular morphogenesis underpinned by the cytoskeleton are associated with tumor progression [15], and many papers addressing cytoskeletal proteins as tumor markers have been published recently [5, 16, 17]. Table 2 focuses on the six cytoskeletal proteins which we identified as upregulated in HCC: actin α/β, filamin-A, talin-1, tubulin α chain, tubulin β chain, and WD repeat-containing protein 1. Actin was identified from 3 peptides significantly upregulated in HCC, and these peptides, SYELPDGQ-VITIGNER, QEYDESGPSIVHR and IWHHTFYNELR, are affiliated with 10, 5 and 7 genes, respectively, of the actin isoforms according to the Swiss-Prot database. Accordingly, the peptide identifications were unable to distinguish among these isoforms. This also is the case for identification of the tu-

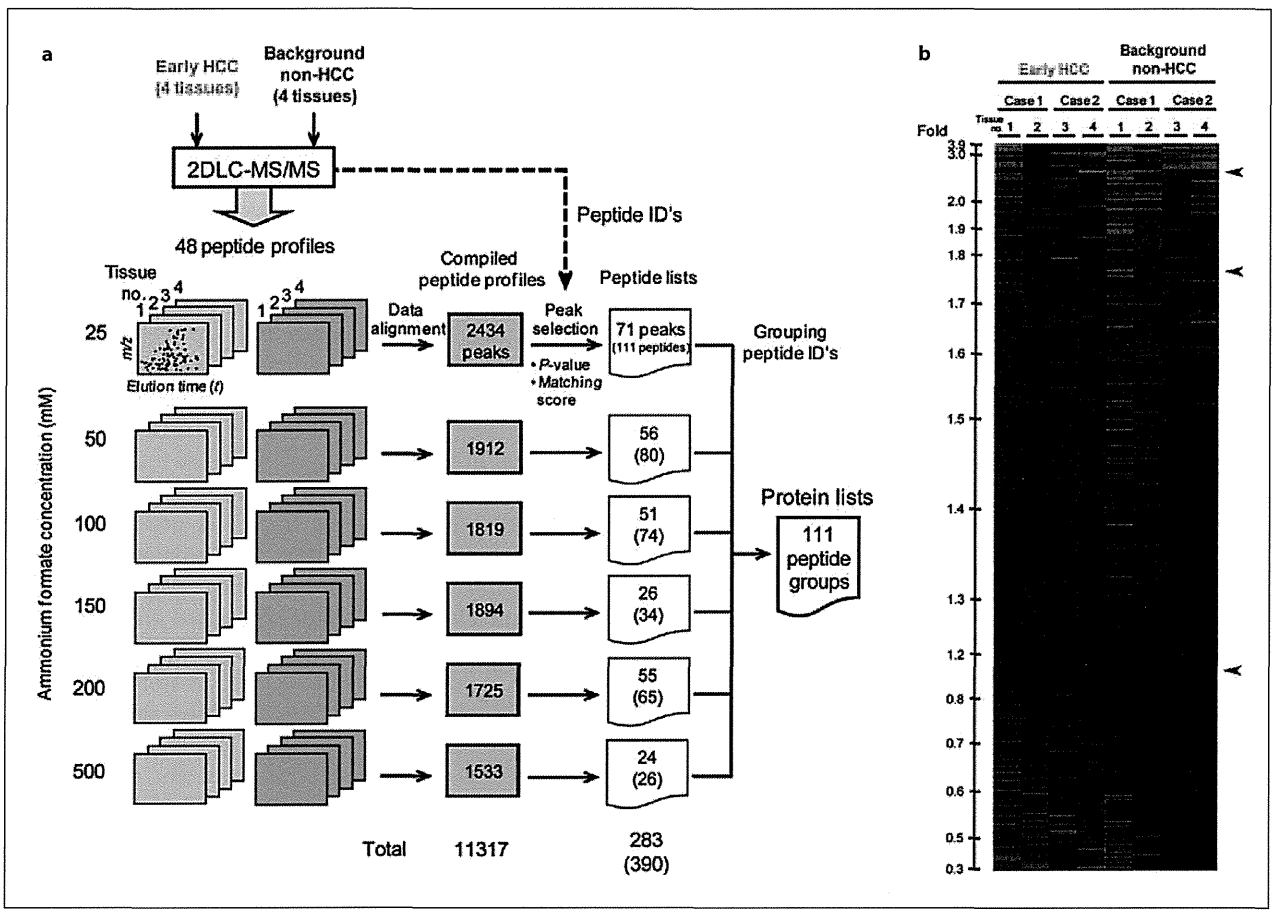

Fig. 1. Proteomic differential analysis using 2DLC-MS/MS. **a** 2DLC-MS/MS of an individual sample generated 6 peptide profiles from SCX LC peptide fractions. The profile data were compiled separately for each SCX LC fraction. This illustration shows the numbers of peaks and peptide identifications in each step. **b** Heat map representation of the 283 peptide peaks. Each color patch represents the ion signal intensity scaled to the mean of signal intensities in the corresponding peptide peak, as a continuum of relative intensity levels from green (less than 0.25-fold of the mean) to bright red (more than 2.5-fold of the mean). These peak data are shown in descending order of the fold value of early HCC to non-HCC. Arrowheads indicate the peak containing a talin-1-derived peptide.

Table 1. Classification of the candidate proteins for HCC tumor marker

Classification	Upregulated	Downregulated	Total
Cytoskeletal protein	6	2	8
Heat shock protein	6	1	7
Major blood protein	3	2	5
Enzyme	39	14	53
Others	7	3	10
Total	61	22	83

Proteins were identified from the peptides whose ion intensities varied significantly between early HCCs and non-HCC tissues ($p < 0.1$). The fold values of early HCC to non-HCC for the peptide ion intensities were used to evaluate the quantitative regulation status of the individual proteins in early HCC.

Table 2. Cytoskeletal proteins upregulated in early HCC

Protein identity (molecular weight, kDa)	Amino acid sequence of peptide	SCX LC salt concentration mM	Mascot ion score[a]	Fold value[b]	p value[c] $\times 10^2$	Swiss-Prot accession (gene name[d])	Number of Swiss-Prot accessions[e]
Actin (42)	SYELPDGQVITIGNER	25	46	1.4	8.95	A5A3E0 (A26C1B), P60709 (ACTB), P62736 (ACTA2), P63261 (ACTG1), P63267 (ACTG2), P68032 (ACTC1), P68133 (ACTA1), Q562R1 (ACTBL2), Q6S8J3 (A26C1A), Q9BYX7 (FKSG30)	10
	QEYDESGPSIVHR	100	35	1.6	2.16	A5A3E0 (A26C1B), P60709 (ACTB), P63261 (ACTG1), Q6S8J3 (A26C1A), Q9BYX7 (FKSG30)	5
	IWHHTFYNELR	200	38	1.4	9.56	A5A3E0 (A26C1B), P60709 (ACTB), P63261 (ACTG1), P68032 (ACTC1), P68133 (ACTA1), Q6S8J3 (A26C1A), Q9BYX7 (FKSG30)	7
Filamin-A (280)	IVGPSGAAVPCK	25	61	1.2	7.10	P21333 (FLNA)	1
Talin-1 (270)	LNEAAAGLNQAATELVQASR	25	35	2.4	3.71	Q9Y490 (TLN1)	1
	VQELGHGCAALVTK	50	35	1.2	4.34	Q9Y490 (TLN1)	1
	LASEAKPAAVAAENEEIGSHIK	100	54	1.7	8.37	Q9Y490 (TLN1)	1
Tubulin α chain (50)	AVFVDLEPTVIDEVR	25	81	1.9	8.43	P68363 (TUBA1B), Q71U36 (TUBA1A), Q9BQE3 (TUBA1C)	3
	AVFVDLEPTVIDEIR	100	70	2.0	2.64	P68366 (TUBA4A)	1
	LISQIVSSITASLR	100	64	1.3	6.70	P68363 (TUBA1B), P68366 (TUBA4A), Q9BQE3 (TUBA1C), Q9H853 (TUBA4B), Q9NY65 (TUBA8)	5
	IHFPLATYAPVISAEK	150	42	1.2	9.75	P68363 (TUBA1B), P68366 (TUBA4A), Q13748 (TUBA3C), Q6PEY2 (TUBA3E), Q71U36 (TUBA1A), Q9BQE3 (TUBA1C)	6
Tubulin β chain (50)	YLTVAAVFR	25	72	1.5	9.68	P04350 (TUBB4), P07437 (TUBB), P68371 (TUBB2C)	3
	SGPFGQIFRPDNFVFGQS GAGNNWAK	200	83	2.3	2.30	P04350 (TUBB4), P07437 (TUBB), P68371 (TUBB2C), Q13885 (TUBB2A), Q9BVA1 (TUBB2B)	5
WD repeat-containing protein 1 (66)	IKDIAWTEDSKR	150	45	1.3	6.76	O75083 (WDR1)	1

[a] The score (S) given as $S = -10 \times \log_{10}(P)$, where P is the absolute probability that the observed match between the MS/MS data and the amino acid sequence is a random event (http://www.matrixscience.com). [b] Signal intensity ratio of early HCC to non-HCC. [c] Significance of the difference between the ion signal intensities of early HCC and non-HCC. [d] The extract from each of the protein entries in Swiss-Prot database of Release 56.1 of September 2, 2008. [e] Protein entries containing the corresponding amino acid sequence.

bulin α and β chains, where the identified peptide sequences belong to 1 or more tubulin isoforms. Identifications of filamin-A and WD repeat-containing protein 1 were supported only by single amino acid sequences. Talin-1 was identified from 3 amino acid sequences, LNEAAAGLNQAATELVQASR, VQELGHGCAALVTK and LASEAKPAAVAAENEEIGSHIK, each being unique in the database. The relevant fold values were 2.4, 1.2 and 1.7, respectively. We focused on talin-1 because of the low ambiguity in both the identification and up-regulation. The real-time quantitative reverse transcription-polymerase chain reaction (RT-PCR) analysis of 3 LDLT cases, including the 2 cases used for the proteomic analysis, also revealed upregulation of talin-1 mRNA in HCC compared to noncancerous liver (data not shown).

Talin-1 Expression in HCC Tissue Samples

The early HCC nodules used for proteomic analyses were stained by the anti-talin-1 antibody with obvious intensity (fig. 2a). Compared with Kupffer cells, vascular smooth muscle cells, bile duct and sinusoidal endothelial

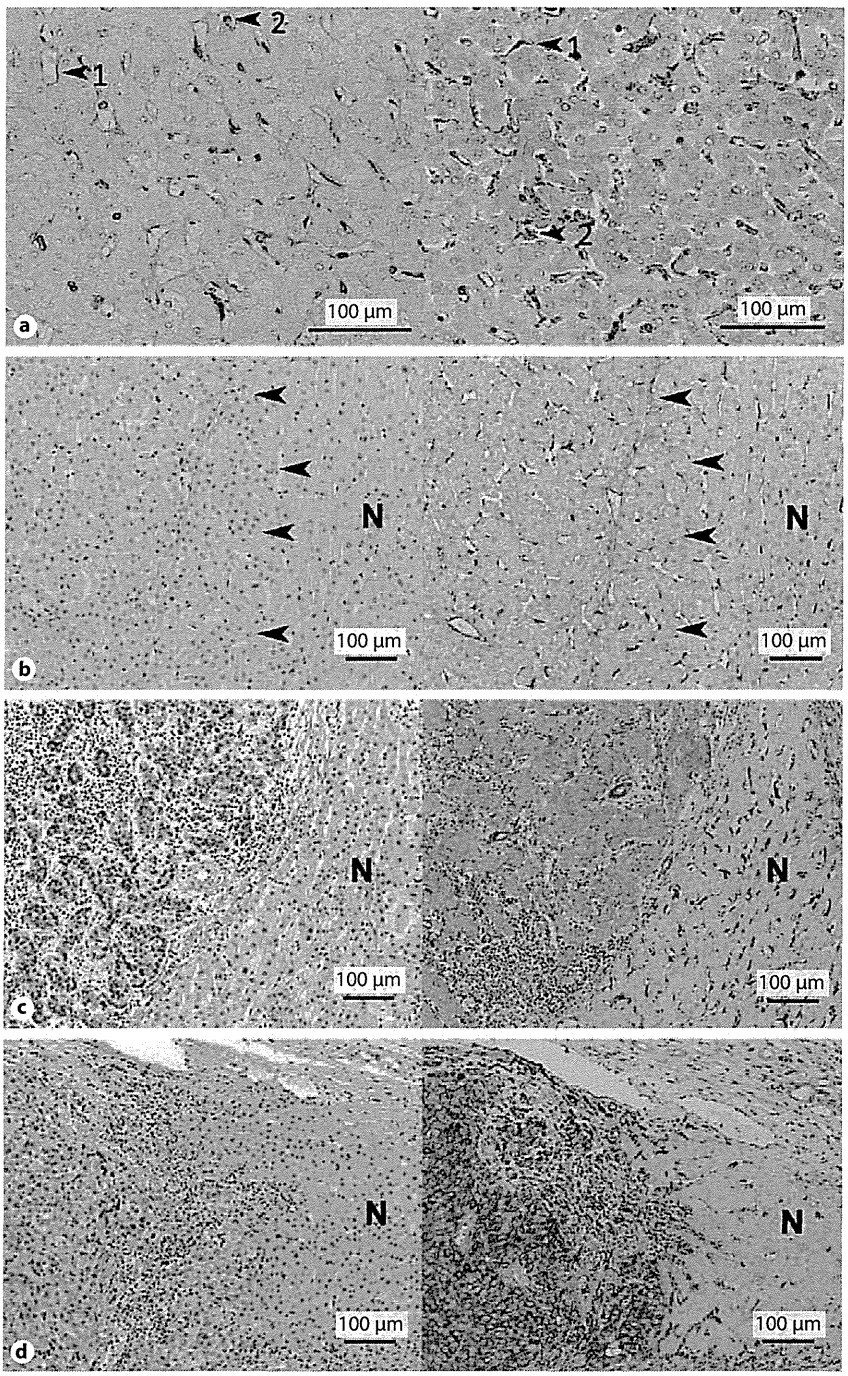

Fig. 2. Immunohistochemical analysis of talin-1. **a** Talin-1 immunostaining of tissue samples used for the proteomic analysis. Left: noncancerous liver tissue. Right: early HCC. Arrowhead 1 indicates a sinusoidal endothelial cell and arrowhead 2 a Kupffer cell. **b–d** Various histological sections were stained with hematoxylin and eosin (left plates) and anti-talin-1 antibody (right plates). **b** An early HCC with slightly stronger staining of talin-1 than the adjacent noncancerous hepatocytes. Arrowheads indicate the borders between early HCC and noncancerous liver (N). **c** A moderately differentiated HCC. **d** A poorly differentiated HCC with very strong staining of talin-1.

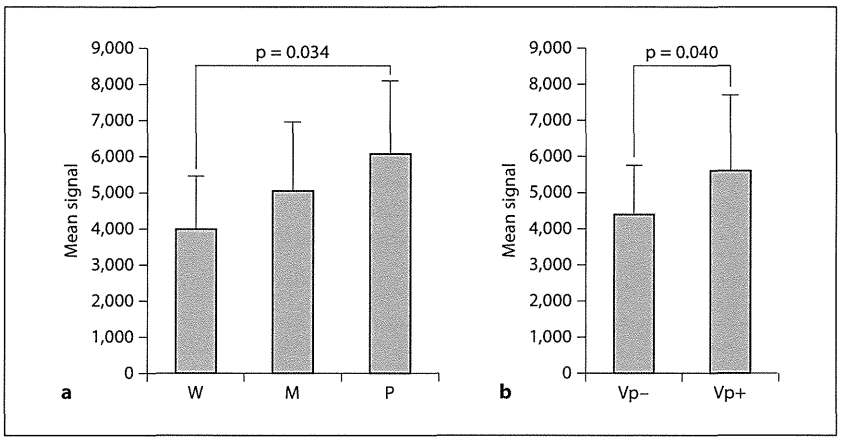

Fig. 3. Microarray analysis. **a** The means of talin-1 mRNA expression in well (W, n = 4), moderately (M, n = 23), and poorly differentiated HCCs (P, n = 13) increased in a stepwise fashion, with a significant difference between well- and poorly differentiated HCCs. **b** The average talin-1 mRNA expression was significantly up-regulated in 28 HCCs with portal vein invasion ('Vp+') as compared to 12 HCCs without portal vein invasion ('Vp–'). Error bars indicate standard deviations.

Table 3. Immunohistochemical reactivity of talin-1 with various histological patterns

Histology	Distribution of the samples according to the percentage of cells with talin-1 upregulation						p value
	<10%	10–30%	30–50%	50–70%	>70%	total	
Dysplastic nodules	4	3	0	1	0	8	
Well-differentiated HCCs (early HCCs)	3 (1)	3 (1)	2 (2)	2 (1)	3 (2)	13 (7)	0.001*
Moderately differentiated HCCs	12	12	11	14	24	73	
Poorly differentiated HCCs	2	0	1	2	15	20	

* Jonckheere-Terpstra test.

cells, which were stained by the anti-talin-1 antibody with remarkable intensity, the immunoreactivity of noncancerous hepatocytes for talin-1 was clearly weak. More intense cytoplasmic staining of the tumor cells by the anti-talin-1 antibody, compared with the adjacent hepatocytes of noncancerous liver, was considered as up-regulation of talin-1 in the tumor cells. The talin-1 immunoreactivities of 8 DNs and 106 HCC nodules are summarized in table 3. Talin-1 was significantly upregulated in early HCC cells compared with adjacent hepatocytes in noncancerous liver (Cochran-Mantel-Haenszel test, p = 0.003). The immunoreactivity of HCCs for talin-1 increased gradually according to the degree of dedifferentiation (fig. 2b–d), with statistical significance (Jonckheere-Terpstra test, p = 0.001). Poorly differentiated HCCs were characterized not only by a high percentage of cancer cells with talin-1 upregulation but also usually by a high intensity of talin-1 staining. DNs were characterized by a significantly lower percentage of talin-1 up-regulation compared with all HCCs together (Cochran-Mantel-Haenszel test, p = 0.003).

We investigated the relationship between clinicopathological factors and the expression of talin-1 (table 4). The mean percentage of HCC cells with talin-1 upregulation in the examined 106 HCC nodules was 53%. We divided HCC samples into 2 groups with either more or less than 50% cancer cells showing talin-1 upregulation. As expected, the degree of cell dedifferentiation differed significantly between the 2 groups (Cochran-Mantel-Haenszel test, p = 0.004). Of great interest was the finding that HCCs containing more than 50% cancer cells with talin-1 upregulation had a significantly higher rate of portal vein invasion (Vp) than those with fewer than 50% cancer cells (Fisher's exact test, p = 0.029). In agreement with these results, the review of our past microarray data [14] showed significant upregulation of talin-1 mRNA in poorly differentiated HCCs compared with well-differentiated HCCs (Student's t test, p = 0.034), as well as in

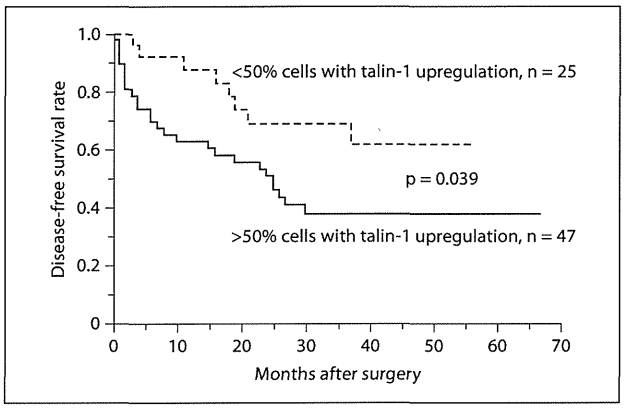

Fig. 4. Kaplan-Meier curves for disease-free survival after surgery. 47 HCC patients with greater talin-1 upregulation (solid line) had a significantly shorter disease-free survival than 25 of those with less talin-1 upregulation (dashed line).

Vp-positive HCCs compared with Vp-negative HCCs ($p = 0.040$) (fig. 3).

During a median follow-up of 25 months (range 0–67), the disease-free survival was analyzed in 72 HCC patients who underwent partial hepatectomy (fig. 4). Setting 50% cancer cells with intense immuno-staining for talin-1 as the threshold, log-rank analysis showed that 47 HCCs with greater talin-1 upregulation had a significantly shorter disease-free survival than 25 of those with less talin-1 upregulation ($p = 0.039$).

Discussion

We applied the latest proteomic technologies to early HCCs and noncancerous tissues derived from native livers of LDLT cases, resulting in identification of talin-1 as a promising candidate marker for HCC progression. In accordance with the proteomic analyses, immunohistochemical examination confirmed talin-1 upregulation in the majority of HCC cells compared with noncancerous hepatocytes. The stepwise increase of immunoreactivity for talin-1 according to the degree of dedifferentiation of HCC suggests the involvement of talin-1 in HCC progression. In general, poor prognosis of progressed HCC is associated with both high rates of intrahepatic metastasis and vascular invasion. The finding that HCCs with upregulation of talin-1 had a significantly higher rate of portal vein invasion might be associated with the shorter time to recurrence after partial hepatectomies for HCCs with talin-1 upregulation, so that the value of talin-1 as a tumor marker may be seen in prediction of clinical outcomes.

Talin-1 is one of several proteins that link the cytoplasmic domains of integrin β subunits to actin filaments [7].

Table 4. Correlations between talin-1 expression and clinical factors

Variables	Distribution of the samples (n[d]) according to the percentage of cells with talin-1 upregulation			p value[e]
	<50%	>50%	total	
Sex				0.599
Male	30	42	72	
Female	6	13	19	
Age				0.510
<60 years	12	23	35	
≥60 years	24	32	56	
Nonviral or viral (HCV + HBV)				0.083
Nonviral	13	10	23	
Viral (HCV + HBV)	23	45	68	
HCV or HBV[a]				0.422
HCV	12	30	42	
HBV	10	15	25	
Background tissue[b]				1.000
Not liver cirrhosis	20	31	51	
Liver cirrhosis	14	22	36	
Histology				0.004
Early/well-differentiated HCC	8	5	13	
Moderately differentiated HCC	35	38	73	
Poorly differentiated HCC	3	17	20	
Portal vein invasion (Vp)[c]				0.029
Vp–	26	21	47	
Vp+	19	39	58	
Intrahepatic metastasis (im)[c]				0.070
im–	38	41	79	
im+	7	19	26	

[a] One case was not counted because of infection with both HCV and HBV. [b] Four cases were not counted because of difficulty in evaluating the histology of the background tissues. [c] One sample was not counted because of difficulty in judging the presence of portal vein invasion and/or intrahepatic metastasis. [d] In the categories 'Sex', 'Age', 'Nonviral or viral', 'HCV or HBV', and 'Background tissue', n indicates the number of cases. When a case had multiple nodules, the highest percentage among the most dedifferentiated nodules was counted. In the categories 'Histology', 'Portal vein invasion', and 'Intrahepatic metastasis', n indicates the number of HCC nodules. [e] All categories were analyzed statistically with Fisher's exact test, except 'Histology' with Cochran-Mantel-Haenszel test.

Binding of talin-1 to β-integrin cytoplasmic domains is thought to trigger a conformational change in the αβ-integrin extracellular domains that increases their affinity for extracellular matrix proteins [18] and promotes assembly of focal adhesions. Talin-1 plays a pivotal role in focal adhesion dynamics, as calpain-2-mediated proteolytic cleavage of talin-1 is a rate-limiting step in focal adhesion disassembly [19]. Interactions between vinculin, talin, and actin filaments appear to constitute a slippage interface between the cytoskeleton and integrins, generating a molecular clutch that is regulated during the morphodynamic transitions of cell migration [20]. Recently, overexpression of talin-1 was reported to promote prostate cancer cell adhesion, migration and invasion [21]. Such knowledge about the cytomorphodynamic roles of talin-1 may be brought in connection with the higher incidence of portal vein invasion in HCCs with talin-1 upregulation. In addition, talin-1 also functions in signal transduction in focal adhesions, as it recruits focal adhesion kinase (FAK), which in turn recruits Src and Ras to activate downstream signaling pathways [22]. It is noteworthy that FAK itself is involved in the metastasis and invasion of HCC [23]. Recently, several molecular-targeted therapies have been developed for the treatment of various malignant diseases, and the multikinase inhibitor sorafenib has shown survival benefits in patients with advanced HCC [24]. Accumulation of knowledge about molecules such as talin-1, which may be involved in carcinogenic signaling pathways, may make available new possibilities for molecular-targeted therapy.

Besides talin-1, the 61 proteins which our proteomic analyses identified as up-regulated in HCC included HSP70, which is known as a molecular marker of HCC [4]. Filamin-A, a cytoskeletal protein listed in table 2, was recently reported to be involved in the metastasis of HCC cells [17]. Our immunohistochemical study, however, did not reveal a significant difference in filamin-A expression between HCC and noncancerous liver (data not shown). The majority of the proteins identified as up-regulated in HCC by our proteomic study still await further validation.

Proteomics has greatly contributed to the identification of specific markers for several human cancers [25]. In this work, we used a high-resolution 2DLC-MS/MS methodology for differential tissue proteome analysis. A characteristic of this strategy lies in the automated alignment of peptide signal data obtained from individual samples, which enables direct comparison of peptide signal intensities among multiple LC-MS/MS runs without any need for isotope labeling [26] and contributes to the increased reliability of analytic results. In addition, proteolytic hydrolysis of the target proteome increases the range of separable protein molecular mass, when compared to the conventional two-dimensional electrophoresis system that is based on the separation of intact proteins by their size/charge and is incapable of detecting high-molecular-mass proteins such as talin-1. It should be noted that perfusion of freshly obtained whole livers with heparinized saline resulted in depletion of body-fluid-derived, high-abundance proteins from the starting materials and, thus, enrichment of tissue proteins in the analyte. With the use of appropriately prepared materials, advanced differential tissue proteomics has the potential to detect quantitative changes of low-abundance tissue proteins which may be the key to carcinogenesis.

In conclusion, talin-1 is significantly upregulated in HCC according to tumor progression and may serve as a prognostic marker. Advanced proteomic techniques applied to freshly obtained whole native livers including early HCC portions may be a powerful method to identify unknown molecules involved in hepatocarcinogenesis.

Acknowledgements

The authors would like to thank Dr. Takeshi Kawamura, Tokyo Medical University, for his insightful supports and comments. Ms. Hisae Anyoji and Mr. Kazuya Wada, Medical Proteo-Scope Co., made enormous contributions to the analysis of the proteomics data. Special thanks also to Mr. Shinji Sato, Maze Inc., Tokyo, Japan, for his technical support of the identical sequence counting.

References

1 Takayama T, Makuuchi M, Hirohashi S, Sakamoto M, Okazaki N, Takayasu K, Kosuge T, Motoo Y, Yamazaki S, Hasegawa H: Malignant transformation of adenomatous hyperplasia to hepatocellular carcinoma. Lancet 1990;336:1150–1153.

2 Takayama T, Makuuchi M, Hirohashi S, Sakamoto M, Yamamoto J, Shimada K, Kosuge T, Okada S, Takayasu K, Yamasaki S: Early hepatocellular carcinoma as an entity with a high rate of surgical cure. Hepatology 1998;28:1241–1246.

3 International Consensus Group for Hepatocellular Neoplasia: Pathologic diagnosis of early hepatocellular carcinoma: a report of the international consensus group for hepatocellular neoplasia. Hepatology 2009;49:658–664.

4 Chuma M, Sakamoto M, Yamazaki K, Ohta T, Ohki M, Asaka M, Hirohashi S: Expression profiling in multistage hepatocarcinogenesis: identification of HSP70 as a molecular marker of early hepatocellular carcinoma. Hepatology 2003;37:198–207.
5 Shibata R, Mori T, Du W, Chuma M, Gotoh M, Shimazu M, Ueda M, Hirohashi S, Sakamoto M: Overexpression of cyclase-associated protein 2 in multistage hepatocarcinogenesis. Clin Cancer Res 2006;12:5363–5368.
6 McDonald WH, Yates JR 3rd: Shotgun proteomics: Integrating technologies to answer biological questions. Curr Opin Mol Ther 2003;5:302–309.
7 Critchley DR: Cytoskeletal proteins talin and vinculin in integrin-mediated adhesion. Biochem Soc Trans 2004;32:831–836.
8 Maeda J, Hirano T, Ogiwara A, Akimoto S, Kawakami T, Fukui Y, Oka T, Gong Y, Guo R, Inada H, Nawa K, Kojika M, Suga Y, Ohira T, Mukai K, Kato H: Proteomic analysis of stage I primary lung adenocarcinoma aimed at individualisation of postoperative therapy. Br J Cancer 2008;98:596–603.
9 Hibi T, Mori T, Fukuma M, Yamazaki K, Hashiguchi A, Yamada T, Tanabe M, Aiura K, Kawakami T, Ogiwara A, Kosuge T, Kitajima M, Kitagawa Y, Sakamoto M: Synuclein-gamma is closely involved in perineural invasion and distant metastasis in mouse models and is a novel prognostic factor in pancreatic cancer. Clin Cancer Res 2009;15:2864–2871.
10 Fujii K, Nakano T, Kanazawa M, Akimoto S, Hirano T, Kato H, Nishimura T: Clinical-scale high-throughput human plasma proteome analysis: lung adenocarcinoma. Proteomics 2005;5:1150–1159.
11 Marko-Varga G, Ogiwara A, Nishimura T, et al: Personalized medicine and proteomics: lessons from non-small cell lung cancer. J Proteome Res 2007;6:2925–2935.
12 Perkins DN, Pappin DJ, Creasy DM, Cottrell JS: Probability-based protein identification by searching sequence databases using mass spectrometry data. Electrophoresis 1999;20:3551–3567.
13 Hsu SM, Raine L, Fanger H: Use of avidin-biotin-peroxidase complex (ABC) in immunoperoxidase techniques: a comparison between ABC and unlabeled antibody (PAP) procedures. J Histochem Cytochem 1981;29:577–580.
14 Chuma M, Saeki N, Yamamoto Y, Ohta T, Asaka M, Hirohashi S, Sakamoto M: Expression profiling in hepatocellular carcinoma with intrahepatic metastasis: Identification of high-mobility group I(Y) protein as a molecular marker of hepatocellular carcinoma metastasis. Keio J Med 2004;53:90–97.
15 Hall A: The cytoskeleton and cancer. Cancer Metastasis Rev 2009;28:5–14.
16 Yamazaki K, Takamura M, Masugi Y, Mori T, Du W, Hibi T, Hiraoka N, Ohta T, Ohki M, Hirohashi S, Sakamoto M: Adenylate cyclase-associated protein 1 overexpressed in pancreatic cancers is involved in cancer cell motility. Lab Invest 2009;89:425–432.
17 Ai J, Huang H, Lv X, Tang Z, Chen M, Chen T, Duan W, Sun H, Li Q, Tan R, Liu Y, Duan J, Yang Y, Wei Y, Li Y, Zhou Q: FLNA and PGK1 are two potential markers for progression in hepatocellular carcinoma. Cell Physiol Biochem 2011;27:207–216.
18 Calderwood DA: Integrin activation. J Cell Sci 2004;117:657–666.
19 Franco SJ, Rodgers MA, Perrin BJ, Han J, Bennin DA, Critchley DR, Huttenlocher A: Calpain-mediated proteolysis of talin regulates adhesion dynamics. Nat Cell Biol 2004;6:977–983.
20 Hu K, Ji L, Applegate KT, Danuser G, Waterman-Storer CM: Differential transmission of actin motion within focal adhesions. Science 2007;315:111–115.
21 Sakamoto S, McCann RO, Dhir R, Kyprianou N: Talin1 promotes tumor invasion and metastasis via focal adhesion signaling and anoikis resistance. Cancer Res 2010;70:1885–95.
22 Chen HC, Appeddu PA, Parsons JT, Hildebrand JD, Schaller MD, Guan JL: Interaction of focal adhesion kinase with cytoskeletal protein talin. J Biol Chem 1995;270:16995–16999.
23 Chen JS, Huang XH, Wang Q, Chen XL, Fu XH, Tan HX, Zhang LJ, Li W, Bi J: FAK is involved in invasion and metastasis of hepatocellular carcinoma. Clin Exp Metastasis 2010;27:71–82.
24 Llovet JM, Bruix J: Molecular targeted therapies in hepatocellular carcinoma. Hepatology 2008;48:1312–1327.
25 Hanash SM, Pitteri SJ, Faca VM: Mining the plasma proteome for cancer biomarkers. Nature 2008;452:571–579.
26 America AH, Cordewener JH: Comparative LC-MS: a landscape of peaks and valleys. Proteomics 2008;8:731–749.

Clinical Study

Oncology

Oncology 2010;79:229–237
DOI: 10.1159/000322374

Received: July 28, 2010
Accepted after revision: September 17, 2010
Published online: March 3, 2011

Significance of DNA Polymerase Delta Catalytic Subunit p125 Induced by Mutant p53 in the Invasive Potential of Human Hepatocellular Carcinoma

Kensaku Sanefuji Akinobu Taketomi Tomohiro Iguchi Keishi Sugimachi Toru Ikegami Yo-ichi Yamashita Tomonobu Gion Yuji Soejima Ken Shirabe Yoshihiko Maehara

Department of Surgery and Science, Graduate School of Medical Sciences, Kyushu University, Fukuoka, Japan

Key Words
Hepatocellular carcinoma · p53 · Invasion · POLD1

Abstract
Objective: To clarify the role of DNA polymerase delta in tumor progression, we examined the expression of its main catalytic subunit p125 encoded by *POLD1* in hepatocellular carcinoma (HCC) and human HCC cell lines. ***Methods:*** We examined the expression of p53 and p125 in HCC by using immunohistochemistry and Western blotting. Characteristic changes observed in human HCC cell lines after transfection were examined. ***Results:*** Immunohistochemical examination revealed positive staining of p125 in HCC cell nuclei, but few positively stained cells were observed in noncancerous tissues ($p < 0.0001$). p125 expression in specimens significantly correlated with cellular differentiation ($p = 0.0048$) and the degree of vascular invasion ($p = 0.0401$). It also significantly correlated with abnormal p53 expression. In vivo studies showed that p125 was upregulated in mutant p53-transfected HepG2 cells, which had more invasive potential than did control cells. Furthermore, the expression and invasive potential were reduced by the silencer sequence for *POLD1*. ***Conclusions:*** These findings suggest that the DNA polymerase delta catalytic subunit p125 induced by mutant type p53 plays an important role in tumor invasion, which leads to a poorer prognosis in HCC.

Introduction

The alpha, delta, and epsilon types of mammalian DNA polymerase are essential for DNA replication [1]. DNA polymerase delta and epsilon regulate the synthesis of the leading and lagging strands, while DNA polymerase alpha is involved in primer synthesis [2] and processes of eukaryotic DNA repair [3, 4]. DNA polymerase delta and epsilon are distinguished from other mammalian DNA polymerases by their intrinsic 3′ to 5′ exonuclease activity which allows them to replicate DNA with high fidelity [5]. DNA polymerase delta replicates a large portion of the genome, synthesizing most of the lagging strand and perhaps contributing to leading-strand synthesis [6, 7].

KARGER

Fax +41 61 306 12 34
E-Mail karger@karger.ch
www.karger.com

0030–2414/10/0794–0229$26.00/0

Accessible online at:
www.karger.com/ocl

Akinobu Taketomi, MD, PhD
Department of Surgery and Science, Graduate School of Medicine, Kyushu University
3-1-1 Maidashi, Higashi-ku, Fukuoka 812-8582 (Japan)
Tel. +81 92 642 5466, Fax +81 92 642 5482
E-Mail taketomi@surg2.med.kyushu-u.ac.jp

The DNA polymerase delta complex consists of 4 subunits: p125, p68, p50, and p12 [8]. The polymerase and the 3′ to 5′ exonuclease active sites of polymerase delta reside in the p125 subunit, which is a 125-kDa protein encoded by *POLD1* in human cells [9]. The *POLD1* promoter is activated by the transcriptional factors Sp1 and Sp2 [9]. Its promoter is also suppressed by wild-type p53 which binds to p53 and recognizes a specific consensus DNA sequence [10]. Sp1 and p53 binding sites overlap each other, and *POLD1* promoter activity therefore appears to be regulated by competition between Sp1 and p53 binding to the site.

The p53 tumor suppressor gene is the most commonly altered protein discovered to date and its product functions as a checkpoint in maintaining genome stability [11]. Inactivation of the p53 gene is essentially due to small mutations that lead to the expression of a mutant protein. The p53 protein is induced and activated in response to various stimuli such as DNA damage or the expression of several oncogenes. p53 activation leads to 1 of 2 major cellular pathways, either apoptosis or cell cycle arrest, which prevents cells from progressing to the S phase until the damaged DNA is fully repaired. p53 recognizes a specific consensus DNA sequence, 5′-PuPuPuC(A/T)(T/A)GPyPyPy-3′, as a transcriptional factor [12].

Hepatocellular carcinoma (HCC) is the fifth most common cancer worldwide and the third most common cause of cancer mortality [13]. Despite recent progress in surgical techniques and postoperative management, the recurrence rates after the surgical resection of HCC remain high [14–17]. p53 overexpression was associated with the histological characteristics of HCC, such as poor cellular differentiation, tumor size, vascular invasion, and poor prognosis [18–21]. It is induced by mutations of the p53 gene, which induce conformational changes to stabilize the protein [22, 23]. These mutations were detected in 27% of HCCs and correlated with cellular differentiation and progression [24].

The following findings were recently reported: (1) defective proofreading of DNA polymerase delta induced a high incidence of epithelial cancers in mice [25]; (2) a *POLD1* variant was associated with an approximately 2-fold increase in the relative risk of breast cancer [26]; (3) the hot spots for the loss of a heterozygosity or allelic imbalance of *BRCA1/2*-related breast cancers harbor *POLD1* [27], and (4) intentional mutation at the polymerase active site of DNA polymerase delta increases genomic instability and accelerates tumorigenesis [28]. DNA polymerase delta is therefore thought to play a crucial role in tumor progression. To clarify the role of DNA polymerase delta in liver cancer, we examined p125 expression in HCC and human HCC cell lines and assessed the characteristic changes in human HCC cell lines observed after transfection and the RNA interference-mediated silencing of p125.

Materials and Methods

Cell Cultures

Three established human lines of HCC and HeLa cells (Riken Cell Bank, Tsukuba, Japan) differing in p53 status were used in this study. Huh7 cells have p53 mutations at codon 220 [29], p53 is deleted in Hep3B cells [30], and HepG2 cells contain wild-type p53 [30]. HeLa cells contain human papilloma virus and wild-type p53. In HeLa cells, any p53 that is synthesized is rapidly degraded by E6 protein, which reduces the level of that protein to 0 [31]. All cells were cultured in DMEM (Life Technologies, Inc.) supplemented with 10% fetal bovine serum, 500 U/ml penicillin, and 500g μg/ml streptomycin (Life Technologies, Inc.), and maintained at 37°C in 5% CO_2.

Patients and Specimens

Tissue samples were obtained from 82 Japanese patients who underwent curative hepatectomy for primary HCC without preoperative treatment at Kyushu University Hospital between 1995 and 2001 and provided preoperative written informed consent. This study conformed to the ethical guidelines of the 1975 Declaration of Helsinki as reflected in a priori approval by the appropriate institutional review committee. All tumors were defined as HCC, and pathological features of the tumors were determined histologically according to the General Rules for the Clinical and Pathological Study of Primary Liver Cancer of the Liver Cancer Study Group of Japan [32].

Quantitative Real-Time Polymerase Chain Reaction

To analyze the mRNA expression, quantitative real-time polymerase chain reactions (qRT-PCR) were performed with a LightCycler® 2.0 system using a Universal Probe Library approach with LightCycler TaqMan Master (Roche, Tokyo, Japan) and appropriate Universal Probes [UPL Probe No. 67 for *POLD1* and No. 60 for glyceraldehyde 3-phosphate dehydrogenase *(GAPDH)*; Roche], according to the manufacturer's instructions. *GAPDH* was used as the internal control. Specific amplification of the target sequence was obtained using primers designed by Probe Finder software (Roche) to amplify *POLD1* (NM_002691.1) or *GAPDH* (NM_002046.3). To verify that the correct targets were amplified, PCR products were run on an agarose gel and visualized with ethidium bromide staining on an ultraviolet transilluminator. The primer sequences for *POLD1* and *GAPDH* were 5′-CCCTACGTGATCATCAGTGC-3′ (forward primer for *POLD1*), 5′-AGGTAGTACTGCGTGTCAATGG-3′ (reverse primer for *POLD1*), 5′-AGCCACATCGCTCAGACA-3′ (forward primer for *GAPDH*), and 5′-GCCCAATACGACCAAATCC-3′ (reverse primer for *GAPDH*).

Western Blot

To analyze protein expression, SDS-PAGE and Western blot were performed using an Invitrogen™ NuPAGE® Novex® Bis-Tris MiniGel system (Invitrogen, Tokyo, Japan) according to the manufacturer's instructions. Normalized protein lysates were boiled in electrophoresis SDS sample buffer, run on a 10% SDS-PAGE gel, and transferred onto a polyvinylidine difluoride membrane (Invitrogen). The primary antibodies used in this study were against p125 (1:200 dilution, mouse monoclonal antibody, clone A-9; Santa Cruz Biotechnology, Inc., Santa Cruz, Calif., USA), p53 (1:1,000 dilution, mouse monoclonal antibody, clone DO-7; Dako, Tokyo, Japan), and β-actin (1:1,000 dilution, mouse monoclonal antibody, clone AC-15; Sigma Aldrich, Tokyo, Japan). Cases in which the relative p125 expression level in the tumor lesion was more than 0.5 [the upper 95% confidence interval (CI) limit of the relative p125 expression level in noncancerous tissues] were considered high-expression cases and the others were considered low-expression cases.

Immunohistochemical Staining

Immunohistochemical observations were performed on adjacent deparaffinized sections using the EnVision™+ System-horseradish peroxidase method (Dako). The primary antibodies used in this study were against p125 (1:300 dilution, rabbit polyclonal antibody, clone H-300; Santa Cruz Biotechnology) and p53 (1:100 dilution, mouse monoclonal antibody, clone DO-7; Dako). Immunohistochemical staining was examined under a light microscope by 2 pathologists. Sections with nuclear staining for p53 in >10% cells were considered positive [20]. Cases in which nuclear staining for p125 was greater in the tumor lesion than in noncancerous tissues were considered high-expression cases and the others were considered low-expression cases.

Invasion Assay

The invasive potential was determined in a Matrigel invasion assay using polycarbonate membranes (pore size 8.0 μm) in the upper chamber of 24-well Transwell culture chambers coated with Matrigel (Becton Dickinson Co., Tokyo, Japan) according to the manufacturer's instructions and as previously described [33]. Cell lines (2.0×10^4 cells/well) suspended in 500 μl DMEM without fetal bovine serum were placed in the upper chamber, and the lower chamber was filled with 750 μl DMEM along with 20% fetal bovine serum as a chemoattractant. Inserts without Matrigel were used as the control. The cells were allowed to migrate through Matrigel for 36 or 72 h. The membranes were stained using a Diff-Quik staining kit (Siemens Healthcare Diagnostics, Inc., Deerfield, Ill., USA). The number of invading cells was expressed as an invasion percentage, i.e. the mean number of cells invading through the Matrigel insert membrane divided by the mean number of cells migrating under the control insert membrane. Each experiment was performed in triplicate.

Plasmid Construction

A p53 Dominant-Negative Vector Set and a pIRES2-AcGFP1 Vector were purchased from Clontech Laboratories, Inc. (Takara Bio). The coding sequence for p53mt135 was ligated into the *Sac*I and *Eco*RI sites of the pIRES2-AcGFP1 vector to generate pIRES2-AcGFP1-p53mt135. The plasmid constructs was confirmed by direct sequence analysis. The pIRES2-AcGFP1-null vector was used as the control. When p53mt135 and p53 are co-expressed, they form a mixed tetramer that is unable to interact with p53-binding sites, thereby blocking the downstream effects of p53 [34, 35].

Stable Transfection

One microgram of plasmid construct was transfected into HepG2 cells using FuGENE® 6 Transfection Reagent (Roche) according to the manufacturer's instructions and as previously described [36]. The transfected cells were selected for resistance to 1,000 μg/ml of G418 (Roche) for 6 weeks. Stably transfected pIRES2-AcGFP1-p53mt135 was confirmed to strongly express p53 by Western blot and by the detection of green fluorescent cells.

RNA Interference

For silencing experiments, cells were transfected with small interfering RNA (siRNA) duplexes using an X-tremeGENE siRNA transfection reagent (Roche), according to the manufacturer's instructions, and harvested 72 h after transfection to obtain the protein. Two siRNAs were purchased from Ambion, Inc. (Applied Biosystems, Tokyo, Japan). Silencer® Negative Control #1 siRNA was used as the negative control. The silencer sequence for *POLD1* was 5′-CCUUCAUCCGUAUCAUGGAtt-3′ (Silencer Select pre-designed siRNA, siRNA ID s614).

Statistical Analysis

Univariate survival analysis was performed using the Kaplan-Meier method and results were compared by univariate logrank and Wilcoxon tests. Metric variables were compared with independent samples by a nonparametric Wilcoxon test. Nominal variables were compared using Fisher and χ^2 tests, and they were compared with multivariate data using multivariate logistic regression analysis. $p < 0.05$ was considered statistically significant. All statistical analyses were performed using JMP 6.0 software for Macintosh (SAS Institute, Inc., Cary, N.C., USA).

Results

p125 Expression in Human HCC

Since p125 expression in clinical samples has not been analyzed before, preliminary analyses of p125 expression levels in human HCC were conducted. Sixty-seven clinical samples (28 noncancerous and 39 cancerous) were examined by Western blot (fig. 1a). p125 expression was significantly higher in human HCC than in noncancerous tissues (fig. 1b; $p < 0.0001$). Immunohistochemistry was performed to identify the cellular localization of p125 in hepatocytes and to determine its expression levels (fig. 1c). There was immunochemical p125 staining in cancer cell nuclei. Few positively stained cells (<1%) were observed in noncancerous tissues. These results show that p125 expression was higher in cancerous tissues than in noncancerous tissues.

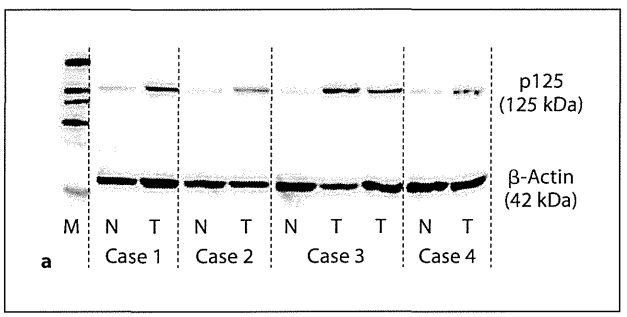

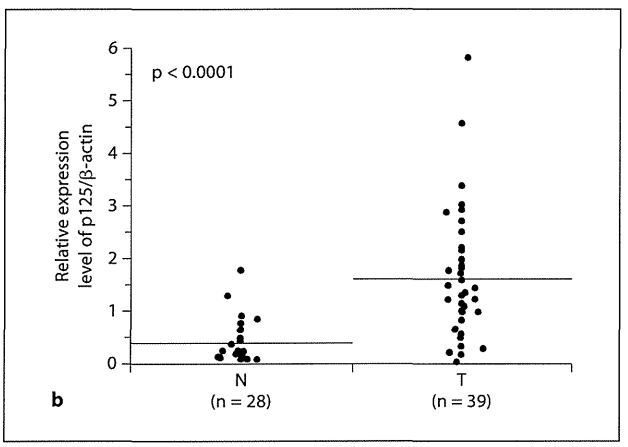

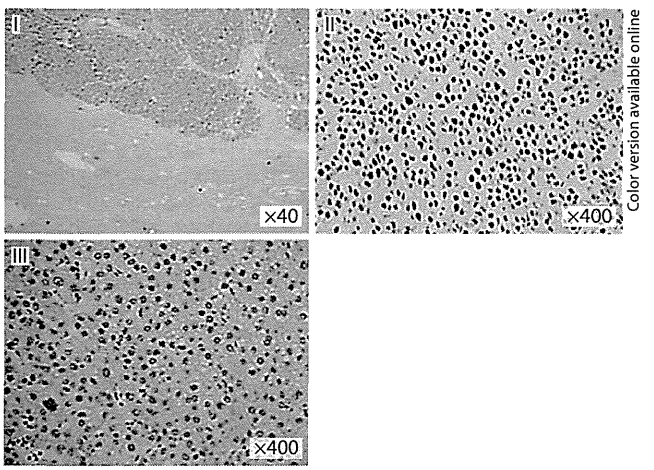

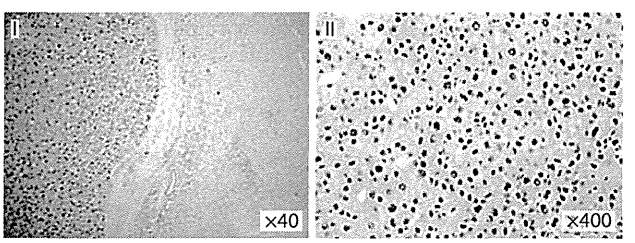

Color version available online

Fig. 1. Immunological expression of p125 and p53 in human HCC. **a** Western blot analysis of p125 in human HCC. Each lane was loaded with 20 μg total protein. **b** Scatter diagram showing the p125 distribution determined by quantitative Western blot in paired normal and tumor liver tissue samples. The relative mean expression level of p125 was 0.38 (95% CI 0.22–0.54) in noncancerous tissues and 1.59 (95% CI 1.19–1.99) in cancerous tissues. **c** Immunohistochemistry for p125. Cases with high p125 expression are shown in I. A cancerous lesion of a case with high p125 expression is shown in II. A cancerous lesion of a case with low p125 expression is shown in III. **d** Immunohistochemistry for p53. A cancerous lesion of a case with p53-positive staining is shown. β-Actin was used as the internal control. M = Marker; N = surrounding normal tissue; T = tumor tissue.

Relationship between the Expression of p125 and POLD1 mRNA

To examine the correlation between the expression of p125 and *POLD1* mRNA, 64 cases were divided into high-expression (n = 46) and low-expression (n = 18) groups based on immunohistochemical findings. mRNA expression was significantly higher in the high-expression group than in the low-expression group (p = 0.0126; fig. 2a). Forty-three cases were divided into 25 high-expression and 18 low-expression cases by Western blot. mRNA expression was significantly higher in high-expression cases than in low-expression cases (p = 0.0164; fig. 2b). These results indicate that p125 expression correlated with *POLD1* mRNA expression.

Relationship between the Expression of p125 and p53

To examine the correlation between the expression of p125 and p53, a total of 82 cases were divided into high-expression (n = 59) and low-expression (n = 23) groups based on immunohistochemical findings for p125. p53 was also stained immunochemically in nuclei (fig. 1d). p53 expression significantly correlated with p125 expression (p = 0.02; fig. 2c). We also examined the p53 mutation of exons 5–8 in 79 cases by direct sequence analysis, excluding 3 cases in which DNA was not available. Immunohistochemical staining of p53-positive cases (47 cases) showed a significantly high p53 mutation rate (28%) compared with p53-negative cases (32 cases, 0%; data not shown). These findings indicate that high p125 expression was associated with abnormal p53 expression.

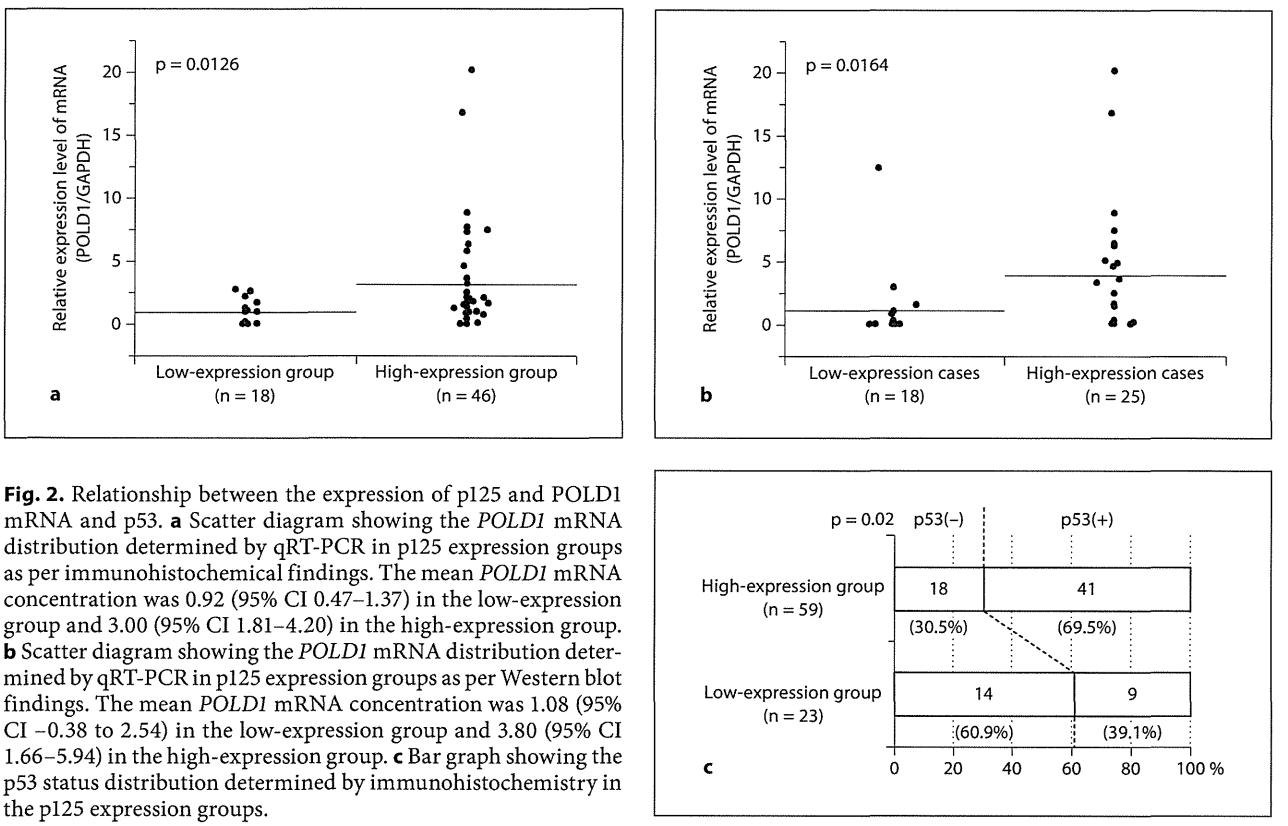

Fig. 2. Relationship between the expression of p125 and POLD1 mRNA and p53. **a** Scatter diagram showing the *POLD1* mRNA distribution determined by qRT-PCR in p125 expression groups as per immunohistochemical findings. The mean *POLD1* mRNA concentration was 0.92 (95% CI 0.47–1.37) in the low-expression group and 3.00 (95% CI 1.81–4.20) in the high-expression group. **b** Scatter diagram showing the *POLD1* mRNA distribution determined by qRT-PCR in p125 expression groups as per Western blot findings. The mean *POLD1* mRNA concentration was 1.08 (95% CI –0.38 to 2.54) in the low-expression group and 3.80 (95% CI 1.66–5.94) in the high-expression group. **c** Bar graph showing the p53 status distribution determined by immunohistochemistry in the p125 expression groups.

Relationship between Immunohistochemical Results, Clinicopathological Features, and Survival

Table 1 shows a comparison of clinicopathological features between patients with tumors expressing high (high-expression group, n = 59) and low (low-expression group, n = 23) p125 levels. p125 expression significantly correlated with gender, the indocyanine green 15-min retention rate, operation time, resection volume, anatomic resection, serum alpha-fetoprotein levels, serum des-gamma-carboxyl prothrombin levels, pathological differentiation, grade, vascular invasion, and intrahepatic metastasis. To examine the association between p125 expression and pathological features, logistic regression for qualitative variables was performed with adjustment for tumor size, tumor number, vascular invasion, intrahepatic metastasis, pathological differentiation, and grade. Backward stepwise multivariate logistic regression analysis revealed that the high p125 expression correlated with poor histological differentiation (p = 0.0048) and positive vascular invasion (p = 0.0401). Survival and disease-free survival were compared between the high- and low-expression groups. The disease-free survival curves of the high- and low-expression groups showed significant separation (p = 0.0496 by Wilcoxon's test; fig. 3).

Relationship between p125 Expression, p53 Expression, and the Invasive Potential of HCC Cell Lines

p125 expression was detected in all HCC cell lines and HeLa cells using Western blot (fig. 4a). Huh7 cells expressed lower p125 levels and higher p53 levels compared with HeLa, HepG2, and Hep3B cells. In p53-deleted Hep3B and rapidly degraded HeLa cells, higher p125 levels were observed. p125 expression and p53 expression were inversely correlated. The invasive potential of those cells was examined using a Matrigel invasion assay (fig. 4b). Huh7 cells exhibited significantly less invasive potential than did the other cell lines ($p < 0.05$). These findings indicate that the invasive potential of HCC cell lines correlated with p125 expression.

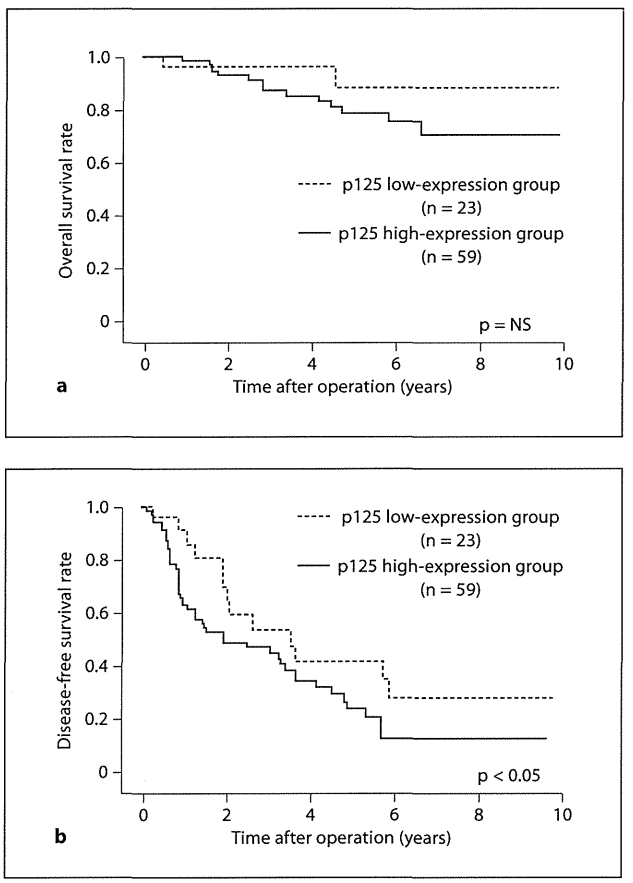

Fig. 3. Survival curves according to p125 expression level. **a** Overall survival curves for HCC patients having tumors with high (solid line) and low expressions (dotted line) of p125 (p = NS). **b** Disease-free survival curves for the high- (solid line) and low-expression (dotted line) groups ($p < 0.05$, Wilcoxon's test).

Table 1. Comparison of clinicopathological features between HCC patients with tumors showing high and low p125 expressions

Variables	p125 expression level		
	low-expression group (n = 23)	high-expression group (n = 59)	p value
Clinical factors			
Age[1], years	65.4 ± 8.5	63.5 ± 9.8	NS
Male/female ratio	22/1	43/16	<0.05
Positive HBs-Ag, %	8.7	20.3	NS
Positive HCV-Ab, %	60.9	66.1	NS
Total protein[1], g/dl	7.2 ± 0.7	7.2 ± 0.7	NS
Albumin[1], g/dl	3.82 ± 0.32	3.85 ± 0.42	NS
AST[1], U/l	52.6 ± 31.2	57.4 ± 25.3	NS
ALT[1], U/l	60.2 ± 41.3	65.8 ± 49.4	NS
Total bilirubin[1], mg/dl	0.81 ± 0.25	0.86 ± 0.33	NS
Platelets[1], $\times 10^4/\mu l$	14.0 ± 4.84	14.2 ± 7.9	NS
PT[1], %	84.8 ± 17.6	82.5 ± 12.2	NS
ICG-R15[1], %	19.5 ± 8.5	15.3 ± 9.0	<0.05
Child's classification (B and C), %	17.4	11.9	NS
Surgical factors			
Operation time[1], min	281 ± 56	330 ± 97	<0.05
Resection volume[1], g	152 ± 153	295 ± 335	<0.05
Anatomical resection, %	26.1	55.9	<0.05
Estimated blood loss[1], g	813 ± 639	1,015 ± 904	NS
Transfusion (+), %	13.0	11.9	NS
Tumor factors			
log[AFP (ng/ml)][1]	1.26 ± 0.88	1.76 ± 1.17	<0.05
log[DCP (mAU/ml)][1]	1.88 ± 0.73	2.39 ± 1.04	<0.05
Tumor size[1], cm	3.04 ± 1.84	4.31 ± 3.12	NS
Tumor number (multiple), %	34.8	44.1	NS
Stage 3 and 4, %	47.8	50.9	NS
Grade 3, %	4.4	28.8	<0.05
Poor histology, %	4.4	30.5	<0.05
Vascular invasion (+), %	0	22.0	<0.05
i.m. (+), %	8.7	32.2	<0.05

[1]Mean ± standard deviation.

HBs-Ag = Hepatitis B virus antigen; HCV-Ab = hepatitis C virus antibody; AST = aspartate aminotransferase; ALT = alanine aminotransferase; PT = prothrombin time; ICG-R15 = indocyanine green 15-min retention test; AFP = alpha-fetoprotein; DCP = des-gamma-carboxyl prothrombin; i.m. = intrahepatic metastasis.

Alteration of the Invasive Potential of HepG2 and p125 Expression

To investigate whether cellular invasiveness was regulated by p125 expression, stable transfection experiments using the induced exogenous dominant negative mutant p53mt135 were performed in HepG2 cells containing wild-type p53. The dominant negative mutant p53mt135 increased p125 expression (fig. 5a). Transfection of the control vector did not affect p125 expression or the invasive potential of HepG2 cells. The latter significantly increased with p125 expression (p = 0.0003; fig. 5b). RNA interference experiments were performed in stably transfected pIRES2-AcGFP1-p53mt135 HepG2 cells using the silencer sequence for *POLD1*. p125 expression was decreased by silencing for *POLD1* transfection (fig. 5c). Negative control siRNA transfection had no effect on p125 expression or its invasive potential. The invasive potential of HepG2 cells was significantly decreased with p125 expression (p = 0.0003; fig. 5d). These findings indicate that the invasive potential directly correlated with p125 expression.

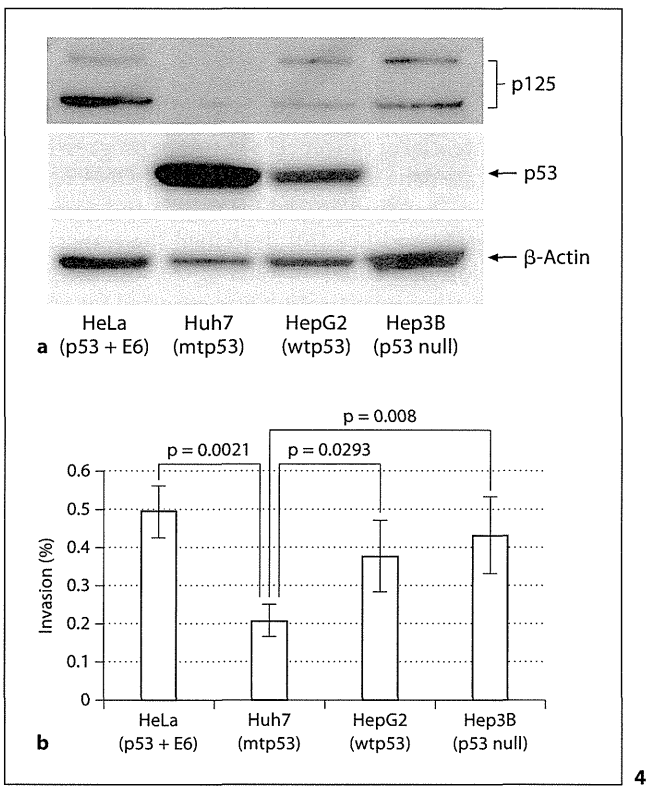

Fig. 4. Relationship between p125 expression, p53 expression, and the invasive potential of HCC cell lines. **a** Western blot of p125 and p53. Each lane was loaded with 20 μg total protein. **b** Invasive potentials were determined by the Matrigel invasion assay. Each experiment was performed in triplicate.

Fig. 5. Alteration of the invasive potential of HepG2 and p125 expression. **a**, **c** Western blot of p125 and p53. Each lane was loaded with 20 μg total protein. **b**, **d** The invasive potential was determined in the Matrigel invasion assay. **b** The mean invasion percentage of nontreated HepG2 cells was set to 1.00 and the invasive potential of stably transfected HepG2 cells is represented as a fraction. **d** The invasion percentage of nontreated stably transfected HepG2 pIRES2-AcGFP1-null cells was calculated as 1.00 and the invasive potential is represented as a fraction. Each experiment shown in **b** and **d** was performed in triplicate.